AD-A162 914 ANALYSIS OF EXPERIMENTAL DATA FOR A 21% THICK NATURAL LAMINAR FLOW AIRFOI..(U) NATIONAL AERONAUTICAL ESTABLISHMENT OTTAWA (ONTARIO) D J JONES ET AL. OCT 85 1/1

UNCLASSIFIED NAE-AN-34 NRC-25076 F/G 20/4 NL

END
FILMED
DTIC

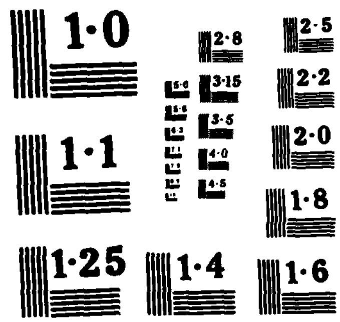

NATIONAL BUREAU OF STANDARDS
MICROCOPY RESOLUTION TEST CHART

UNLIMITED
UNCLASSIFIED

Canada

ANALYSIS OF EXPERIMENTAL DATA FOR A 21% THICK NATURAL LAMINAR FLOW AIRFOIL, NAE 68-060-21:1

by

D.J. Jones, M. Khalid
National Aeronautical Establishment

OTTAWA
OCTOBER 1985

AERONAUTICAL NOTE
NAE-AN-34
NRC NO. 25076

National Research Council Canada
Conseil national de recherches Canada

NATIONAL AERONAUTICAL ESTABLISHMENT

SCIENTIFIC AND TECHNICAL PUBLICATIONS

AERONAUTICAL REPORTS:

Aeronautical Reports (LR): Scientific and technical information pertaining to aeronautics considered important, complete, and a lasting contribution to existing knowledge.

Mechanical Engineering Reports (MS): Scientific and technical information pertaining to investigations outside aeronautics considered important, complete, and a lasting contribution to existing knowledge.

AERONAUTICAL NOTES (AN): Information less broad in scope but nevertheless of importance as a contribution to existing knowledge.

LABORATORY TECHNICAL REPORTS (LTR): Information receiving limited distribution because of preliminary data, security classification, proprietary, or other reasons.

Details on the availability of these publications may be obtained from:

Publications Section,
National Research Council Canada,
National Aeronautical Establishment,
Bldg. M-16, Room 204,
Montreal Road,
Ottawa, Ontario
K1A 0R6

ÉTABLISSEMENT AÉRONAUTIQUE NATIONAL

PUBLICATIONS SCIENTIFIQUES ET TECHNIQUES

RAPPORTS D'AÉRONAUTIQUE

Rapports d'aéronautique (LR): Informations scientifiques et techniques touchant l'aéronautique jugées importantes, complètes et durables en termes de contribution aux connaissances actuelles.

Rapports de génie mécanique (MS): Informations scientifiques et techniques sur la recherche externe à l'aéronautique jugées importantes, complètes et durables en termes de contribution aux connaissances actuelles.

CAHIERS D'AÉRONAUTIQUE (AN): Informations de moindre portée mais importantes en termes d'accroissement des connaissances.

RAPPORTS TECHNIQUES DE LABORATOIRE (LTR): Informations peu disséminées pour des raisons d'usage secret, de droit de propriété ou autres ou parce qu'elles constituent des données préliminaires.

Les publications ci-dessus peuvent être obtenues à l'adresse suivante:

Section des publications
Conseil national de recherches Canada
Établissement aéronautique national
Im. M-16, pièce 204
Chemin de Montréal
Ottawa (Ontario)
K1A 0R6

UNLIMITED
UNCLASSIFIED

ANALYSIS OF EXPERIMENTAL DATA FOR A 21% THICK NATURAL LAMINAR FLOW AIRFOIL, NAE 68-060-21:1

ANALYSE DE DONNÉES EXPÉRIMENTALS D'UN PROFIL AÉRODYNAMIQUE À ÉCOULEMENT LAMINAIRE NATUREL, NAE 68-060-21:1, D'UNE ÉPAISSEUR DE 21%

by/par

D.J. Jones, M. Khalid

National Aeronautical Establishment

AERONAUTICAL NOTE
NAE-AN-34
NRC NO. 25076

OTTAWA
OCTOBER 1985

L.H. Ohman, Head/Chef
High Speed Aerodynamics Laboratory/
Laboratoire d'aérodynamique à hautes vitesses

G.M. Lindberg
Director/Directeur

SUMMARY

NAE and de Havilland Aircraft of Canada have designed and tested in the NAE 5 ft X 5 ft wind tunnel a 21% thick supercritical airfoil capable of sustaining long runs of laminar flow on both surfaces. The measured drag levels are superior to those of any model previously tested in this facility and are comparable to classical NACA and modern NASA NLF airfoils.

RÉSUMÉ

NAE et de Havilland Aircraft of Canada ont conçu et testé dans la soufflerie aérodynamique NAE 5 pi X 5 pi un profil supercritique d'une épaisseur de 21% capable de maintenir de longs trajets d'écoulement laminaire sur ses deux surfaces. Les niveaux de trainée mesurés sont supérieurs à ceux de tous les modèles testés précédemment dans ces installations et sont comparables aux profils NACA classiques et NASA NLF modernes.

CONTENTS

		Page
	SUMMARY	(iii)
	SYMBOLS	(vi)
1.0	INTRODUCTION	1
2.0	LIFT CHARACTERISTICS	2
	2.1 A Discussion of $C_L - \alpha$	2
	2.2 Lift Performance	3
3.0	A DISCUSSION OF $C_M - \alpha$	3
4.0	AIRFOIL DRAG	4
	4.1 A Discussion of Wake Drag	4
	4.2 Drag Comparison Against Other Airfoils	6
5.0	PRESSURE DISTRIBUTIONS	6
	5.1 A Comparison With Theoretical Computations	6
	5.2 Experimental Pressure Behaviour	7
6.0	CONCLUSIONS	7
7.0	REFERENCES	7

TABLE

Table		Page
1	A Summary of Parameters C_{D_W} and $C_{D_{W_2}}$	9

ILLUSTRATIONS

Figure		Page
1	C_L and C_M versus α, $R_c \simeq 12.8 \times 10^6$, $M_\infty = 0.3, 0.5$ and 0.6	11
2	C_L and C_M versus α, $R_c \simeq 12.8 \times 10^6$, $M_\infty = 0.66, 0.68, 0.70$	12
3	C_L and C_M versus α, $M_\infty = 0.3$, $R_c \simeq 6.8$ and 12.8×10^6	13
4	C_L and C_M versus α, $M_\infty = 0.6$, $R_c \simeq 6.8$ and 12.8×10^6	14
5	C_L and C_M versus α, $M_\infty = 0.3$, $R_c \simeq 6.8$ and 12.8×10^6	15

ILLUSTRATIONS (Cont'd)

Figure		Page
6	C_L and C_M versus α, $R_c \simeq 6.8 \times 10^6$, $M_\infty = 0.68$	16
7	$\partial C_L/\partial\alpha$ versus Free Stream Mach Number	17
8	Lift Performance at $R_c = 6.8 \times 10^6$	18
9	Lift Performance at $R_c = 12.8$ and 16.7×10^6	19
10	The Wake Rake Probe Locations Relative to the Airfoil	20
11a	C_{D_W} versus C_{L_B} for $M_\infty = 0.3$	21
11b	$C_{D_{W_2}}$ versus C_{L_B} for $M_\infty = 0.3$	22
12a	C_{D_W} versus C_{L_B} for $M_\infty = 0.6$	23
12b	$C_{D_{W_2}}$ versus C_{L_B} for $M_\infty = 0.6$	24
13a	C_{D_W} versus C_{L_B} for $M_\infty = 0.7$	25
13b	$C_{D_{W_2}}$ versus C_{L_B} for $M_\infty = 0.7$	26
14a	C_{D_W} versus C_{L_B} for $M_\infty = 0.3$, 0.5 and 0.6	27
14b	$C_{D_{W_2}}$ versus C_{L_B} for $M_\infty = 0.3$, 0.5 and 0.6	28
15a	C_{D_W} versus C_{L_B} for $M_\infty = 0.66$, 0.68 and 0.70	29
15b	$C_{D_{W_2}}$ versus C_{L_B} for $M_\infty = 0.66$, 0.68 and 0.70	30
16a	$C_{D_{W_2}}$ versus M_∞ for $C_L = 0.3$	31
16b	C_{D_W} versus M_∞ for $C_L = 0.3$	32
17a	$C_{D_{W_2}}$ versus M_∞ for $C_L = 0.5$	33
17b	C_{D_W} versus M_∞ for $C_L = 0.5$	34
18a	$C_{D_{W_2}}$ versus M_∞ for $C_L = 0.6$	35
18b	C_{D_W} versus M_∞ for $C_L = 0.6$	36
19a	$C_{D_{W_2}}$ versus M_∞ for $C_L = 0.7$	37
19b	C_{D_W} versus M_∞ for $C_L = 0.7$	38
20a	Range Parameter $M_\infty C_L/C_{D_W}$ Values for $R_c = 6.8 \times 10^6$	39
20b	Range Parameter $M_\infty C_L/C_{D_W}$ Values for $R_c = 12.8 \times 10^6$	40

ILLUSTRATIONS (Cont'd)

Figure		Page
20c	Range Parameter $M_\infty C_L/C_{D_W}$ Values for $R_c = 16.7 \times 10^6$	41
21a	Drag Comparisons With Other Airfoils Using C_{D_W}	42
21b	Drag Comparisons With Other Airfoils Using $C_{D_{W_2}}$	43
22	Comparison Between Theory and Experiment $M_\infty = 0.68$, $C_L = 0.623$, $R_c = 12.8 \times 10^6$	44
23	To Show the Effect of Different Transition Points on the BGK Pressure Distribution $M_\infty = 0.68$, $C_L = 0.623$, $R_c = 12.8 \times 10^6$	45
24a	Drag Count Levels for Various Positions of Transition (Theoretical) $R_c = 12.8 \times 10^6$, $M_\infty = 0.68$, $C_L = 0.6$	46
24b	Drag Count Levels for Various Positions of Transition (Theoretical) $R_c = 6.8 \times 10^6$, $M_\infty = 0.68$, $C_L = 0.6$	46
25	Effect of R_c on the Pressure Distribution	47
26	Effect of Increasing M_∞ on the C_p Distribution	48

SYMBOLS

Symbol	Definition
M	Mach number
C_L	lift coefficient
$C_{L_{sep}}$	lift coefficient at which separation first starts to occur
C_M	pitching moment about quarter chord, negative nose down
C_{D_W}	drag measured by the wake rake and averaged from probes 1 and 3 (see Fig. 10)
$C_{D_{W_2}}$	drag measured from probe 2
$C_{D_{W_3}}$	drag measured from probe 3
R_c	Reynolds number based on a 10 in. chord
α	angle of attack (corrected for wall interference)
M_{DR}	drag rise Mach number
Subscripts	
B	taken from balance measurements
∞	free stream (free stream Mach number is corrected for wall interference)
max	maximum value

ANALYSIS OF EXPERIMENTAL DATA FOR A 21% THICK NATURAL LAMINAR FLOW AIRFOIL, NAE 68-060-21:1

1.0 INTRODUCTION

As part of an ongoing study of supercritical wing sections carried out jointly by NAE and de Havilland*, we present here some results obtained from wind tunnel tests on a 21% thick airfoil. Other airfoils in the series are 16% thick (see Ref. 1) and shortly will include 13% and 10% thick sections. The main objective of the present design is to investigate the possibility of achieving long runs of laminar flow on both the upper and lower surfaces. It was thought this would be difficult in the NAE 5 ft X 5 ft blowdown wind tunnel since it is not a low turbulence tunnel and the effect of the free stream turbulence on transition was uncertain.

The study of Natural Laminar Flow (NLF) airfoils has been in progress worldwide for many years but it has always been difficult to achieve good NLF results in real flight due to imperfections in the wing surfaces. Recently there has been a more sustained interest in the NLF concept, particularly in the United States, as modern manufacturing methods and materials yield much improved wing surfaces. Unfortunately most of the modern work is classified and so comparisons of our own work in this field with others is difficult. Only at low speed (Somers, Refs. 2 and 3) are other results available and comparisons are made in Reference 1 which show that our drag levels, at supercritical Mach numbers, are very similar to drag at low speed, reported by Somers, in the Langley low turbulence tunnel.

The NLF concept for achieving low drag is only one method amongst many others such as suction and energizing of boundary layers on aerodynamic surfaces, Reference 4, wavy surfaces, Reference 5, augmentor airfoils, Reference 6, large eddy break-up devices, Reference 7, turbulence manipulators, Reference 8.

The computational method employed in our design was the well known BGK Computer code[9] modified to include Green's boundary layer method. The non-conservative option was used as this gives a better correlation with experiment. A slightly favourable but fairly flat upper surface pressure distribution up to the shock was sought at the design condition ($M_\infty = 0.68$, $C_L = 0.6$) while on the lower surface a quite favourable gradient up to minimum pressure at about 40% chord was sought. A modest aft loading was also a criterion but with pitching moments not too high. These conditions were met using the BGK code with transition fixed at the standard 7 and 15% locations on the upper and lower surfaces. It is demonstrated that a reasonable agreement is obtained between this theoretical pressure distribution and that obtained from the experiment. In the experiment one must remember that the pressure holes themselves cause turbulence and so the measured pressure distribution, in a turbulent chordwise strip, is presumably not representative of the NLF pressure distribution on the remainder of the airfoil. Thus any prediction of the NLF pressure distribution cannot be verified under present conditions but would need unobtrusive measurement techniques. Alternatively two models, one with staggered pressure holes, could be used. The BGK prediction of pressures with a free transition option developed by de Havilland shows a more favourable distribution on the upper surface and a less favourable one on the lower surface compared to 7 and 15% transition points. It also shows more aft loading but the same shock strength.

Our studies also show that as the free stream Mach number increases through supercritical, at the design lift say, the upper surface pressure gradients become more favourable as the shock gets stronger. Thus it seems that more and more laminar flow is possible on the upper surface yielding lower drags until eventually the wave drag dominates the situation and drag rise appears. Hence most of our drag plots show fairly extensive buckets covering a ΔM of up to 0.04. They also show a sharp drag rise after the bucket which may be due to laminar flow separation.

---

* with support from NRC PILP project CA155-1-0655/252

It is also shown that fully turbulent drag levels (one of the wake rake probes was directly in line with the pressure tappings) are of a reasonable size and are quite comparable with other supercritical airfoils.

Other experimental data on thick supercritical airfoils is rather scarce. Van Egmond and Rozendal[10] report on an 18% thick airfoil (NLR 7501) tested in the NLR pilot tunnel at Mach numbers of about 0.73 but at low Reynolds number (about 2 million). In terms of drag, with free transition, they found a narrow drag bucket at $M_\infty = 0.765$ (uncorrected) with $C_L \simeq 0.4$ which is the 'tunnel design condition'. The drag here was about 100 counts rapidly rising to 120 counts for $\Delta M_\infty \simeq \pm 0.01$. The authors assessed the narrow bucket as being due to flow separation for a slight variation from the design condition. The design of this airfoil was not favourable to long runs of laminar flow with pressure peaks on the upper and lower surfaces being at about 7% and 5% respectively.

Blackwell (Ref. 11) presented data on supercritical airfoils of 10, 16 and 21% maximum thickness. He was particularly looking at Reynolds number scale effects. With regard to the 21% airfoil, suitable for span loader type aircraft, data was presented for Reynolds numbers of 7, 11 and 22 million. For a Mach number of 0.68 and C_L about 0.65 it was shown that the drag decreased from about 0.0183 to 0.0163 as Reynolds number increased from 7 to 22 million. In this case transition was probably at about 10% on the upper surface and 40% on the lower surface judging from the pressure distribution. Quite strong shocks were present on the upper surface and the flow went supercritical on the lower surface. Blackwell states this was not an optimum design and later Lockheed developed a 20% thick optimized airfoil which is classified[12].

In our 21% airfoil case it will be seen that, contrary to the above, drag increases over the Reynolds number range covered, that is from 7×10^6 to 17×10^6. This is presumably due to the fact that we have a fairly constant transition Reynolds number so that transition will be further forward on the foil as R_c is increased. Thus there is less laminar flow and hence higher drag as R_c increases.

The design conditions for the present foil were $M_\infty = 0.68$ with $C_L = 0.6$. Three Reynolds numbers (based on a 10 inch chord) of 6.8, 12.8 and 16.7 were used in the experimental tests which were carried out in the NAE 5 ft $\times$ 5 ft blowdown wind tunnel. A data report (Ref. 13) describes the operating conditions, the equipment and the measurements taken in this test. The analysis of the measurements is the subject of this report.

2.0 LIFT CHARACTERISTICS

2.1 A Discussion of C_L-α

In all our discussions of lift and moments we decided to use balance measurements as these better represent laminar flow conditions rather than pressure integrated values. In actual fact the two readings did not give significantly different values.

Two types of graph are presented in this discussion. In the first set, Figures 1 and 2, Reynolds number R_c (based on chord) is held constant whilst the Mach number is changed. In the second set, Figures 3 and 4, the converse is true.

The pitching moment shown in the above figures will be dealt with later.

The constant Reynolds number graphs of Figures 1 and 2 show that increasing the Mach number has the effect of increasing $\partial C_L/\partial\alpha$ in the linear part of these curves. It changes gradually from a low value of $\partial C_L/\partial\alpha = 0.116$ at $M_\infty = 0.3$ to $\partial C_L/\partial\alpha = 0.2$ at $M_\infty = 0.7$. Figures 1 and 2 also show that in order to obtain the design $C_{L_B} = 0.6$ at constant $R_c = 12.7 \times 10^6$, in the Mach number range $0.3 \leqslant M_\infty \leqslant 0.7$, the angle of attack must correspondingly reduce from 1.718 to 0.5°. The zero incidence lift coefficient $C_{L_{\alpha=0}}$ also increases with increasing Mach number from a low of about $C_{L_B} = 0.4$, at $M_\infty = 0.3$ to a peak of $C_{L_B} = 0.513$ at $M_\infty = 0.68$.

The three plots in Figures 3 to 5 show the effect of changing the Reynolds number whilst the Mach number is held constant. It seems that on the linear portion of the C_{L_B} versus α curve the Reynolds number change has small effect, except at $M_\infty = 0.7$ (Fig. 5) where the lower R_c case produces significantly more lift. It can be seen from these figures that, as expected, C_L is quite linear up to stall onset. Beyond this point the stall is well behaved and does not produce any rapid loss of lift.

The $C_{L_{max}}$ obtained is very much a function of the Mach number. The highest $C_{L_{max}}$ value obtained was about 1.7 at $M_\infty = 0.3$, $R_c = 6.84 \times 10^6$ at $\alpha = 13.75°$ shown in Figure 3. At the design Mach number $M_\infty = 0.68$, and $R_c = 12.87 \times 10^6$ the $C_{L_{max}}$ obtained was about 0.95 at $\alpha = 3.4°$ as seen in Figure 2. By relaxing the Reynolds number down to $R_c = 6.83 \times 10^6$, C_L reaches a maximum value of about 1.0 at $\alpha = 7.4°$, see Figure 6.

Finally on Figure 7 we show the variation of $\partial C_L/\partial\alpha$ against free stream Mach number. These values are practically identical for both $R_c = 6.8$ and 12.8×10^6; there is insufficient data at $R_c = 16.7 \times 10^6$. Also shown is the Prandtl Glauert curve for $\partial C_L/\partial\alpha$.

2.2 Lift Performance

Figures 8 and 9 show the lift performance against Mach number at low ($R_c = 6.8 \times 10^6$) and high Reynolds number ($R_c = 12.8 \times 10^6$, 16.7×10^6) respectively. The upper curve in both figures corresponds to the $C_{L_{max}}$ obtained from the lift-incidence curves, whilst the lower curve corresponds to $C_{L_{sep}}$. $C_{L_{sep}}$ is obtained by a de Havilland procedure of plotting C_p versus C_L at a chord station $x/c = 0.96$, and then determining the point on the curve where $\partial C_p/\partial C_L = -0.4$ (Ref. 14). Lift corresponding to the drag rise Mach numbers was also determined from appropriate drag polars, as explained later, and is shown in both figures.

In both figures it is apparent that $C_{L_{max}}$ and $C_{L_{sep}}$ generally diminish as Mach number increases. At the lower Reynolds number $R_c = 6.8 \times 10^6$, (Fig. 8) the rate of decay of $C_{L_{max}}$ and $C_{L_{sep}}$ from a high of 1.69 and 1.58 respectively at $M_\infty = 0.3$ to a low of 0.85 and 0.48 is less orderly compared to the high Reynolds number case in Figure 9. Note the large gap between $C_{L_{max}}$ and $C_{L_{sep}}$ at $M_\infty = 0.5$ in Figure 8. Both Reynolds numbers show a converging of $C_{L_{max}}$ and $C_{L_{sep}}$ in the region $0.64 \leqslant M_\infty \leqslant 0.66$. At design Mach number $M_\infty = 0.68$, both figures show values of $C_{L_{max}} = 1.0$ and $C_{L_{sep}} = 0.9$.

Very little data was available for $R_c = 16.7 \times 10^6$.

3.0 A DISCUSSION OF $C_M - \alpha$

At low Mach number in the range 0.3 to 0.6, $R_c = 12.7 \times 10^6$, the pitching moment C_{M_B} (referenced to ¼ - chord) shows very small variations with α, Figure 1. For the range where C_{L_B} is less than $C_{L_{max}}$ the value of C_{M_B} lies in the range $0.11 \leqslant |C_{M_B}| \leqslant 0.135$. At the higher Mach number range $M_\infty = 0.66$ to 0.7 in Figure 2, there seems to be somewhat of a linear trend of C_{M_B} against α in the range $-2 \leqslant \alpha° \leqslant 1.50$. The $\partial C_M/\partial\alpha$ value is about -0.005, yielding an aerodynamic centre of about 0.03 i.e. 28% chord.

At Mach numbers 0.3 and 0.6, in Figures 3 and 4, respectively, the pitching moment is not affected significantly by changing the Reynolds number from 6.8×10^6 to 12.8×10^6. At the higher Mach number $M_\infty = 0.7$ (Fig. 5), the difference in C_{M_B} values for the same Reynolds number change is quite measurable. The values of C_{M_B} at the lowest Mach number $M_\infty = 0.3$ in Figure 3 remain well behaved within the range $0.1 \leqslant |C_{M_B}| \leqslant 0.125$. At higher Mach numbers $M_\infty = 0.6$ and 0.7 in Figures 4 and 5 respectively, C_{M_B} displays a weak sinusoidal relationship with α. The static damping coefficient $\partial C_{M_B}/\partial\alpha$ has values of -0.006 for $M_\infty = 0.6$ (Figure 4), and -0.01 at $M_\infty = 0.7$ (Figure 5) for small angles of attack.

4.0 AIRFOIL DRAG

4.1 A Discussion of Wake Drag

The wake drag was measured by the standard sidewall-mounted traversing rake supporting four pitot probes. The method is based on measuring the momentum defect in the wake, see Reference 15 for instrumentation and method. The signal from probe 4 is ignored as it is sometimes affected by the disturbed sidewall boundary layer. Ordinarily the total effective drag C_{D_W} is computed from an average of the remaining three probes. However, in this experiment the second probe (probe 2) lined up exactly downstream of the chordwise pressure taps on the model surface (see Fig. 10). This was at first thought to be a bad choice in that one probe, with reading from a turbulent strip, would be useless. However on second thoughts it was realized that the readings could be useful for giving turbulent drag levels more typical of a conventional aircraft with imperfection on the wings. Some background of our design ideas here will be useful.

The design of the 21% airfoil was done in such a way as to capitalize upon long runs of laminar flow on both the upper and lower surfaces. This was achieved by pressure gradients favourable enough to overcome the slight imperfections or dust always present on a model surface. To aid the latter problem the model was cleaned between runs. However, as mentioned, the pressure taps themselves gave a problem since they produced premature transition and turbulence.

With the above in mind a comparison of drag from Probe 2, $C_{D_{W_2}}$, is made against the average drag from Probes 1 and 3 denoted C_{D_W}. As expected the former is larger — often by a considerable amount. This is illustrated in Figures 11 to 15. In particular the 'fully turbulent' drag is 50 counts higher than the 'natural laminar flow' drag at design conditions ($M_\infty = 0.68$, $C_L = 0.6$).

Figures 16a and 16b, respectively show $C_{D_{W_2}}$ and C_{D_W} against Mach number for Reynolds numbers (R_c) 6.8×10^6, 12.8×10^6 and 16.7×10^6, at $C_L = 0.3$. $C_{D_{W_2}}$ in Figure 16a shows a continuously increasing trend against Mach number up to $M_\infty = 0.64$, after which the low Reynolds number ($R_c = 7 \times 10^6$) curve begins to diminish describing a bucket with a minimum value of about $C_{D_{W_2}} = 0.0110$ at $M_\infty = 0.685$. The higher Reynolds number curve maintains its upward trend, increasing sharply from a value of $C_{D_{W_2}} = 0.013$ at $M_\infty = 0.66$ to $C_{D_{W_2}} = 0.017$ at $M_\infty = 0.68$ and then dropping back to about $C_{D_{W_2}} = 0.0148$ at $M_\infty = 0.7$. The reason for this behaviour is not apparent. At $R_c = 16.7 \times 10^6$ only three points were measured, and they indicate an increase in $C_{D_{W_2}}$ from 0.0108 to 0.0130 between $M_\infty = 0.66$ and 0.7.

The corresponding drag as obtained from C_{D_W} for the above three Reynolds numbers at $C_L = 0.3$ is smaller and shows more distinctly a bucket, see Figure 16b. Generally the curves indicate a decrease in drag coefficient up to $M_\infty = 0.6$. Beyond this point, there is a mild increase up to $M_\infty = 0.66$ after which the bucket phenomenon is observed. The drag at the low Reynolds number ($R_c = 6.8 \times 10^6$) dips as low as $C_{D_W} = 0.0057$ at $M_\infty = 0.68$. At $R_c = 12.8 \times 10^6$, this minimum bucket point has a value of about $C_{D_W} = 0.0065$ at $M_\infty = 0.685$. At the high Reynolds number $R_c = 16.7 \times 10^6$, the three data points also demonstrate the bucket effect giving a minimum $C_{D_W} = 0.0099$ at $M_\infty = 0.68$.

Two approaches are adopted to evaluate the drag rise Mach number, M_{DR}. One method is based on determining the point on the Drag versus Mach number graph where $\partial C_D/\partial M = 0.1$. The second method involves adding 20 drag counts to the average of the lower Mach number C_{D_W} values, and finding the point on the rising branch of the curve which corresponds to this drag value. The drag rise Mach number on each curve for the above two methods is appropriately shown. The two methods give different values of M_{DR} as can be judged by inspecting any one curve. For instance, M_{DR} based on $\partial C_D/\partial M = 0.1$ for $R_c = 6.8 \times 10^6$ in Figure 16b is 0.708, and based on the 20 counts approach M_{DR} is 0.720.

As expected, the two drags, (C_{D_W} and $C_{D_{W_2}}$) yield different M_{DR}. For example, the M_{DR} values based on the $\partial C_D/\partial M = 0.1$ method for $C_{D_{W_2}}$ at 6.8×10^6 is $M_{DR} = 0.696$. The corresponding M_{DR} value for C_{D_W} is $M_{DR} = 0.708$ for the same R_c.

Figures 17a and 17b show a similar comparison of $C_{D_{W_2}}$ and C_{D_W} for $C_L = 0.5$. Once again there is a similar behaviour. $C_{D_{W_2}}$ again shows a mild peak at 0.011 for $R_c = 6.8 \times 10^6$ and $M_\infty = 0.64$ followed by a moderate bucket with $C_{D_{W_2}}$ minimum of 0.0104 at $M_\infty = 0.662$. Even at the higher Reynolds number $R_c = 12.8 \times 10^6$ there is a vague gesture of a bucket with $C_{D_{W_2}}$ minimum of about 0.0114 at $M_\infty = 0.68$. The C_{D_W} versus M_∞ graph at $C_L = 0.5$ in Figure 17b shows a gentle decrease up to 0.6 (up to 0.66 for $R_c = 6.8 \times 10^6$). All three Reynolds numbers tested confirm the bucket type decrease in drag. C_{D_W} for the Mach number range $0.66 \leqslant M_\infty \leqslant 0.72$. A minimum value of $C_{D_W} = 0.0057$ was observed at $M_\infty = 0.68$ for $R_c = 6.8 \times 10^6$. Once again the drag rise Mach number values from both methods are shown in the figures.

This theme of two types of drag ($C_{D_{W_2}}$ and C_{D_W}) comparison is continued in Figures 18a and 18b respectively for a $C_L = 0.6$. $C_{D_{W_2}}$ in Figure 18a, after an upward trend against Mach number is showing more of a pronounced bucket for $R_c = 6.8 \times 10^6$ in the Mach number range $0.64 \leqslant M_\infty \leqslant 0.71$ with a minimum $C_{D_{W_2}}$ value of about 0.0109. The higher Reynolds number, $R_c = 12.8 \times 10^6$, curve however shows somewhat of an inflexion region at $M_\infty = 0.66$ and $C_{D_{W_2}} = 0.0130$ and continues to grow for higher Mach number values. Also included with the curves of Figure 18a are the results from the BGK computer code for $R_c = 15 \times 10^6$ which do not show any bucketing which is to be expected since transition is fixed at 7 and 15% on the upper and lower surfaces. The corresponding drag results C_{D_W} are shown in Figure 18b. There is little change in drag up to $M_\infty = 0.6$. The higher Reynolds number $R_c = 12.8 \times 10^6$ curve shows some peaking at $M_\infty = 0.6$ before dropping with the 'bucket' minimum value of 0.0082 at $M_\infty = 0.68$. But the low Reynolds number curve continues to diminish beyond $M_\infty = 0.6$ with the rate of decrease intensifying after $M_\infty = 0.66$ as it enters the bucket behaviour to give a $C_{D_W} = 0.0064$ at $M_\infty = 0.695$. This figure also shows differences between C_{D_W} and $C_{D_{W_3}}$ which are typical also at other conditions.

Note that the difference in drag rise Mach number M_{DR}, as given by the two methods is very small. It lies in the limits $0.7 \leqslant M_{DR} \leqslant 0.704$ based on $\partial C_D/\partial M = 0.1$ method and in the range $0.706 \leqslant M_{DR} \leqslant 0.71$ based on 20 counts approach.

Figures 19a and 19b compare $C_{D_{W_2}}$ and C_{D_W} at a C_L of 0.7. The overall drag behaviour in different Mach number regimes is very similar to the previous cases. Note the uptrend in C_{D_W} at $M_\infty = 0.64$ before entering the bucket in the Mach boundary $0.64 \leqslant M_\infty \leqslant 0.7$. A minimum C_{D_W} value of about 0.0072 was recorded at the bottom of the bucket for $R_c = 6.8 \times 10^6$ at $M_\infty = 0.68$. At $R_c = 12.8 \times 10^6$, this value of minimum C_{D_W} has risen to 0.0085 for the same Mach number $M_\infty = 0.68$.

For $C_{D_{W_2}}$, Figure 19a shows the presence of a drag bucket in the region $0.64 \leqslant M_\infty \leqslant 0.7$, after showing a peak at 0.64. The minimum value of drag in the bucket is about 0.0114 at $M_\infty = 0.664$. $C_{D_{W_2}}$ does not show any buckets at higher Reynold numbers.

An explanation of the drag buckets mentioned above will be made when we study pressure distributions in a later section.

Finally we show values of the range parameter $M_\infty C_L/C_{D_W}$ on Figure 20. It is interesting to note that for all three Reynolds numbers the maximum range parameter is predicted at a higher C_L than design. The maximum is at $M_\infty = 0.68$ and $0.7 < C_L < 0.8$ approximately.

Note that surface roughness does not seem to have been a factor in triggering transition as our surface roughness has an RMS value of about 15×10^{-6} inches compared to a laminar boundary layer displacement thickness of about 10^{-3} inches at mid chord.

Table 1 summarizes the findings of this section. Note that the drag values are exceptionally good compared to other airfoil sections particularly in view of the fact that this foil is 21% maximum thickness. A comparison with other airfoils will now be made.

4.2 Drag Comparison Against Other Airfoils

The drag of the current 21% thickness airfoil is significantly lower than other foils tested at NAE (except for the 16% thickness foil from the same family of foils). On inspection of Figure 21a we see that Hoerner's (Ref. 16) fully turbulent shock free drag curve provides a representative low boundary for most of the foils. Note that some of the foils used fixed transition strips and thus lost the advantage of natural laminar flow (NLF). However, some of the foils using NLF still showed drag levels comparable with those of fixed transition. This could have been due to unfavourable pressure gradients (as in the 'peaky' type airfoils) or could be due to tunnel turbulence levels at the time of testing. Recent improvements (Ref. 17) to the NAE 5 ft × 5 ft wind tunnel might have cleaned up some of this turbulence. Thus our current 16% and 21% foils may be taking fuller advantage of NLF.

Also shown on Figures 21a and 21b are 18% and 24% t/c augmentor wing (multi-element airfoil) data as taken from Reference 18.

It can be seen that both 16% and 21% foils show excellent drag levels at $R = 8 \times 10^6$/ft while at 15×10^6/ft the 21% still performs remarkably well and the 16% is very good. Even at 20×10^6/ft the 21% is only just giving a drag value above that of Hoerner's.

Other comparisons of the current 21% airfoil (as well as our 16%) are made in Reference 1. In that reference it is demonstrated that our airfoil, at design Mach number, has drag levels comparable to NASA NLF airfoils at $M_\infty \simeq 0.1$.

Besides comparing the NLF drag levels with other airfoils it is also useful to compare the turbulent drag levels recorded on probe 2, namely $C_{D_{W_2}}$. This value may be more representative of true flight conditions and so ideally we require a low drag level here also. On inspecting Figure 21b we see that our drag levels are very good compared to other single and multi-element airfoils with the 8 and 20×10^6 Reynolds number values only just above Hoerner's curve.

5.0 PRESSURE DISTRIBUTIONS

5.1 A Comparison With Theoretical Computations

Comparison of experimental and theoretical pressure distributions can only be meaningful in our case if we fix transition in the calculation quite near to the leading edge. This has to be done since, as mentioned, the pressure holdes themselves cause turbulence and lie in a turbulent strip of the otherwise laminar flow airfoil. The theory used here is the BGK non-conservative code[9] with Green's boundary layer method. A comparison near the design point is made in Figure 22 and shows a reasonably good agreement. The next figure[23] shows the effect of moving the transition point on both the upper and lower surfaces back to near the minimum pressure values on each surface. It can be seen that the pressure distributions are quite different and that the pressure becomes more favourable as the transition point moves back while at the same time the shock strength remains constant with $M_\infty(\text{shock}) \simeq 1.17$. The aft loading is increased. This increase in aft loading will be investigated in future tests when some pressure holes aft of 60% will be placed at a different spanwise location on the airfoil.

The drag values, for $M_\infty = 0.68$ and $C_L = 0.6$, for different theoretical locations of transition are shown in Figures 24a and 24b. As expected the drag differences are very significant. Our experimental drag is also shown as a locus on the figures. As can be seen, correlation of experimental drag with the theoretical values obtained with natural transition is difficult as the higher Reynolds number case yields a lower drag (0.0045) than the lower Reynolds number case (0.0057). This is opposite to the experimental observation (0.0082 and 0.0071).

Another attempt at a correlation can be made if we adjust upward the theoretical drag levels by 22 counts (found from previous correlations on airfoils with smaller runs of laminar flow). To observe this correlation we have plotted on Figures 24 the locus of the experimental drag levels minus 22 counts. It can be seen from Figure 24b, at $R_c = 6.8 \times 10^6$, that a reasonable prediction of drag could be made by assuming about 65% and 40% transition points for the upper and lower surfaces respectively. At $R_c = 12.8 \times 10^6$, Figure 24a, the indication is that transition would be closer to 50% and 30% respectively.

5.2 Experimental Pressure Behaviour

The effect of Reynolds number on the pressure distribution is shown in Figure 25. Remembering that these pressure taps are in a turbulent boundary layer it is not surprising that the pressures are virtually independent of Reynolds number. One can only surmise that had the pressure measurements been taken in the presence of the natural laminar boundary layer the distributions would have been different due to the different lengths of laminar flow.

The difference in pressure distributions as Mach number is increased for a constant lift of roughly 0.65 is shown in Figure 26. Assuming that at least the trends of this turbulent pressure distribution are similar to the NLF trends we can conclude that as M_∞ increases the pressure is becoming more favourable to longer runs of laminar flow. This must be the reason for the drag bucket mentioned earlier.

6.0 CONCLUSIONS

At the lower Reynolds number of 6.8×10^6 it appears that long runs of laminar flow are possible producing very low drag values. The length of this flow diminishes as Reynolds number is increased until at 16.7×10^6 drag levels are comparable to other "turbulent flow" airfoils tested at NAE.

Because of the success of this airfoil and of a similar 16% design (Ref. 1) further investigations will be made on thinner airfoil sections which will exploit natural laminar flow.

7.0 REFERENCES

1. Eggleston, B.; Jones, D.J. — *The Development of Thick, Low Drag Supercritical Airfoils.* Canadian Aeronautics and Space Institute Journal. To be published 1986.

2. Somers, D.M. — *Design and Experimental Results for a Natural Laminar Flow Airfoil for General Aviation Application.* NASA TP-1861.

3. Somers, D.M. — *Design and Experimental Results for a Flapped Natural Laminar Flow Airfoil for General Aviation Applications.* NASA TP-1865, June 1981.

4. Shinichi, Y. — *Experimental Study of Turbulent Flow Near a Suction Tube.* AIAA J. 18, 2, 1980, p.p. 222-223.

5. Cary, A.M. Jr.; Weinstein, L.M.; Bushnell, D.M. — *Drag Reduction Characteristics of Small Amplitude Rigid Surface Waves.* Symposium on Viscous Drag Reduction, November 1979.

6. Whittley, D.C. — *An Update on the Canada/USA Augmentor-Wing Concept.* Agard CPP365, May 1984.

7. Bertelrud, A.
Truong, T.V.
Avellan, F.
Drag Reduction in Turbulent Boundary Layers Using Ribbons.
AIAA Paper 82-1370.

8. Bushnell, D.M.
Anders, J.B.
Walsh, M.J.
McInville, R.V.
Turbulent Drag Reduction Research.
Agard CPP365, May 1984.

9. Bauer, F.
Garabedian, P.
Korn, D.
Supercritical Wing Sections III.
Lecture Notes in Economics and Mathematical Systems, No. 150.
Springer-Verlag 1977.

10. van Egmond, J.A.
Rozendal, D.
The Design and Aerodynamic Characteristics of an 18% Thick Shock Free Airfoil (NLR 7501).
NLR Report NLR MP 78016 U, 1978.

11. Blackwell, J.A. Jr.
Scale Effects on Supercritical Airfoils.
ICAS Conference Proceedings, Vol. 1, 1978.

12. Hinson, B.L.
Blackwell, J.A. Jr.
Design and Wind Tunnel Test of a 20% Thick Supercritical Airfoil at Transonic Speeds.
NASA CR-145118, Jan. 1977 (Classified).

13. Khalid, M.
Jones, D.J.
Experimental Investigation of a 21% Thick Supercritical Airfoil NAE 68-060-21:1 in the 15" X 60" Facility.
NAE Report LTR-HA-5X5/0155, March 1985 (Confidential).

14. Eggleston, B.
Jones, D.J.
Elfstrom, G.M.
Development of Modern Airfoil Sections for High Subsonic Cruise Speeds.
Atlantic Aeronautical Conference, March 1979.

15. Ohman, L.H.
The NAE 15" X 60" Two Dimensional Test Facility; New Features and Some Related Observations, Results of New Centre Line Calibration at 20.5% Porosity.
NRC Report LTR-HA-15, 1973.

16. Hoerner, S.F.
Fluid Dynamic Drag.
1965.

17. Ohman, L.H.
Brown, D.
Bowker, A.J.
Ellis, F.A.
Recent Improvements to the NAE 5 ft X 5 ft Blowdown Wind Tunnel.
NRC Report AN-31, 1985.

18. Whittley, D.C.
An Update of the Canada/USA Augmentor-Wing Project.
AGARD-CP-365, 1984.

TABLE 1

A SUMMARY OF PARAMETERS C_{D_W} AND $C_{D_{W_2}}$

C_{D_W}

CONDITIONS	$10^{-6} R_c$	$C_L = 0.3$	$C_L = 0.5$	$C_L = 0.6$	$C_L = 0.7$
Bucket Region	7	$0.66 \leq M_\infty \leq 0.712$	$0.66 \leq M_\infty \leq 0.712$	$0.66 \leq M_\infty \leq 0.710$	$0.64 \leq M_\infty \leq 0.710$
	13	$0.66 \leq M_\infty \leq 0.718$	$0.66 \leq M_\infty \leq 0.710$	$0.66 \leq M_\infty \leq 0.700$	—
	17	$0.66 \leq M_\infty \leq 0.700$	$0.66 \leq M_\infty \leq 0.696$	—	—
Bucket Min Drag	7	0.0057	0.0057	0.0064	0.0072
	13	0.0065	0.0079	0.0082	0.0085
	17	0.0099	0.0099	0.0110	—
M_{DR} based on $\partial C_D/\partial M_\infty = 0.1$	7	0.708	0.703	0.700	0.692
	13	0.704	0.703	0.687	0.688
	17	—	0.699	—	0.690
M_{DR} based on 20 counts	7	0.720	0.719	0.710	—
	13	0.722	0.716	0.700	0.700
	17	—	—	—	—

$C_{D_{W_2}}$

CONDITIONS	$10^{-6} R_c$	$C_L = 0.3$	$C_L = 0.5$	$C_L = 0.6$	$C_L = 0.7$
Bucket Region	7	$0.64 \leq M_\infty \leq 0.700$	$0.64 \leq M_\infty \leq 0.686$	$0.64 \leq M_\infty \leq 0.704$	$0.64 \leq M_\infty \leq 0.696$
	13	—	$0.66 \leq M_\infty \leq 0.686$	—	—
	17	—	—	—	—
Bucket Min Drag	7	0.0110	0.0104	0.0109	0.0114
	13	—	0.0114	—	—
	17	—	—	—	—
M_{DR} based on $\partial C_D/\partial M_\infty = 0.1$	7	0.696	0.694	0.704	0.699
	13	0.662	0.690	0.700	0.690
	17	—	—	—	—
M_{DR} based on 20 counts	7	0.702	0.694	0.706	—
	13	0.624	0.690	0.657	0.682
	17	—	—	—	—

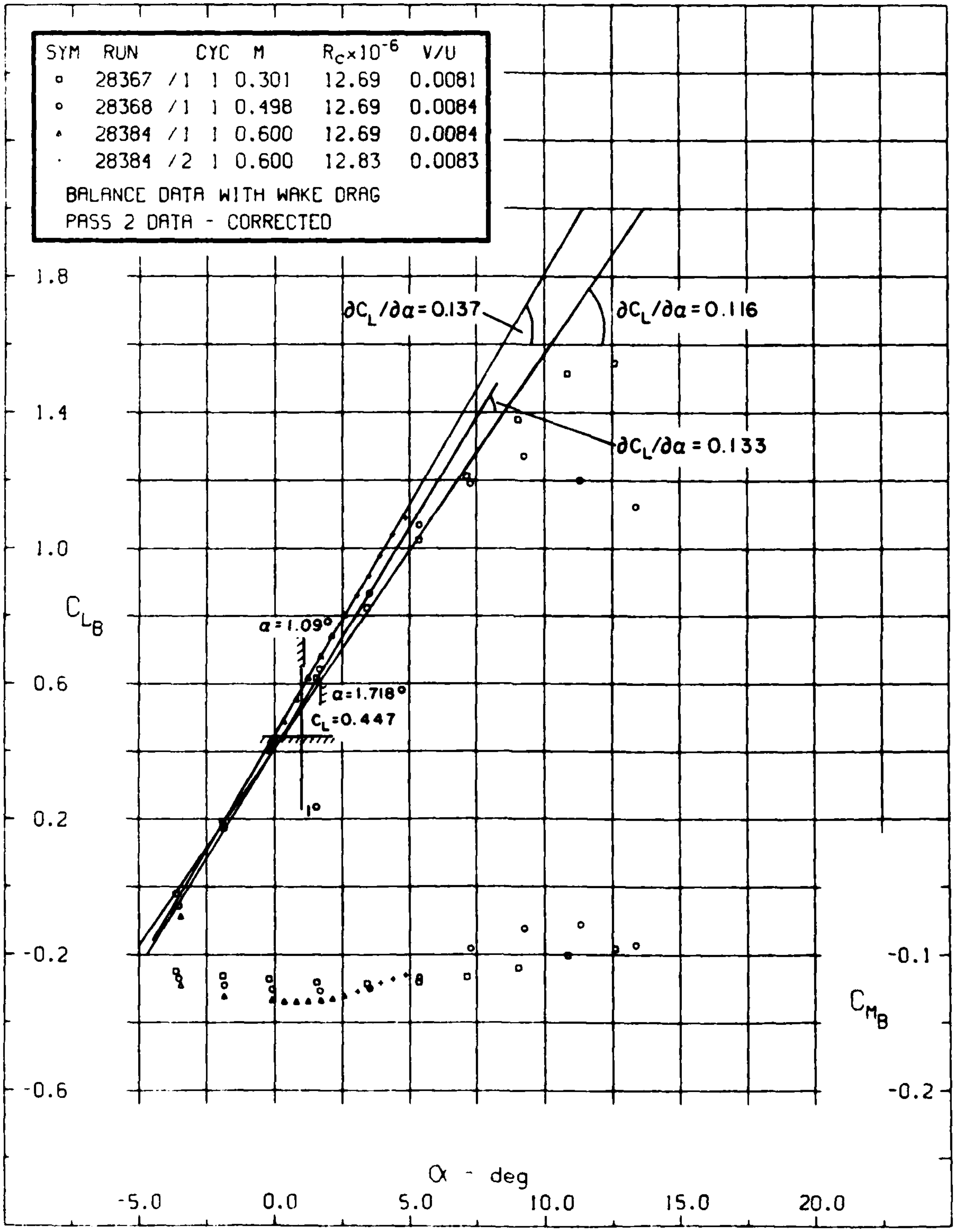

FIG. 1: C_L AND C_M VERSUS α, $R_c \simeq 12.8 \times 10^6$, M_∞ = 0.3, 0.5 AND 0.6

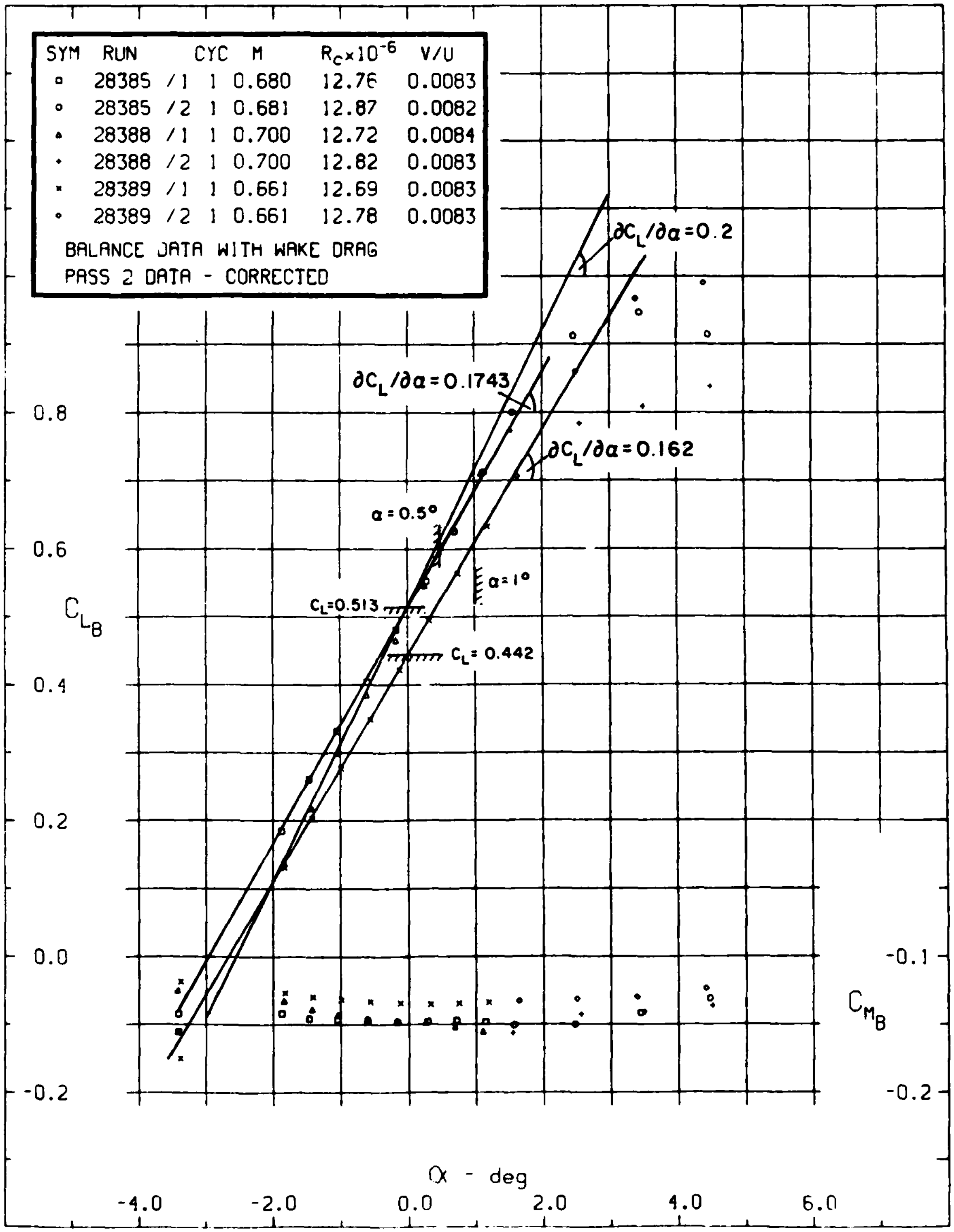

FIG. 2: C_L AND C_M VERSUS α, $R_c \simeq 12.8 \times 10^6$, $M_\infty = 0.66, 0.68, 0.70$
DIFFERENT SCALE TO FIG. 1

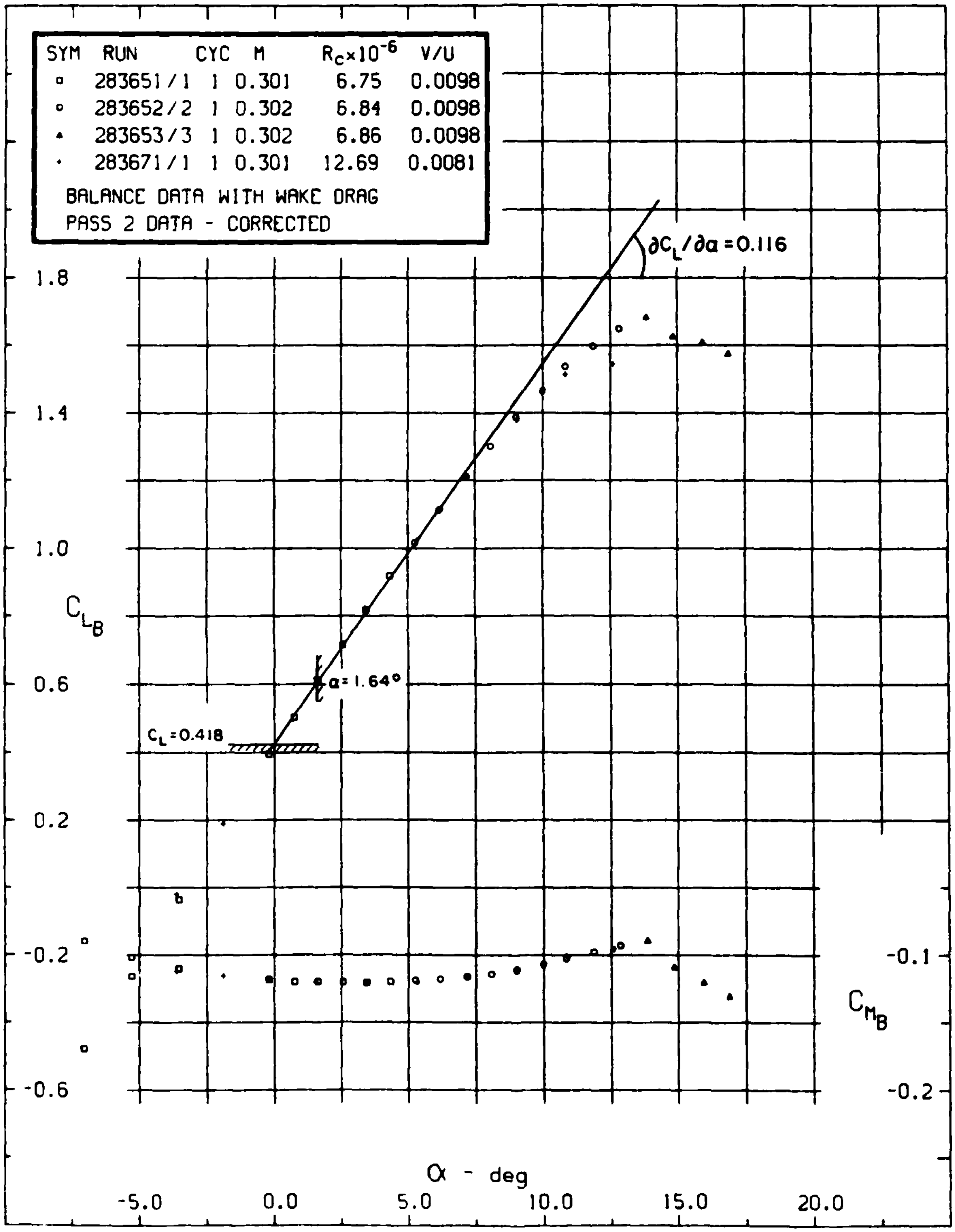

FIG. 3: C_L AND C_M VERSUS α, $M_\infty = 0.3$, $R_c \simeq 6.8$ AND 12.8×10^6

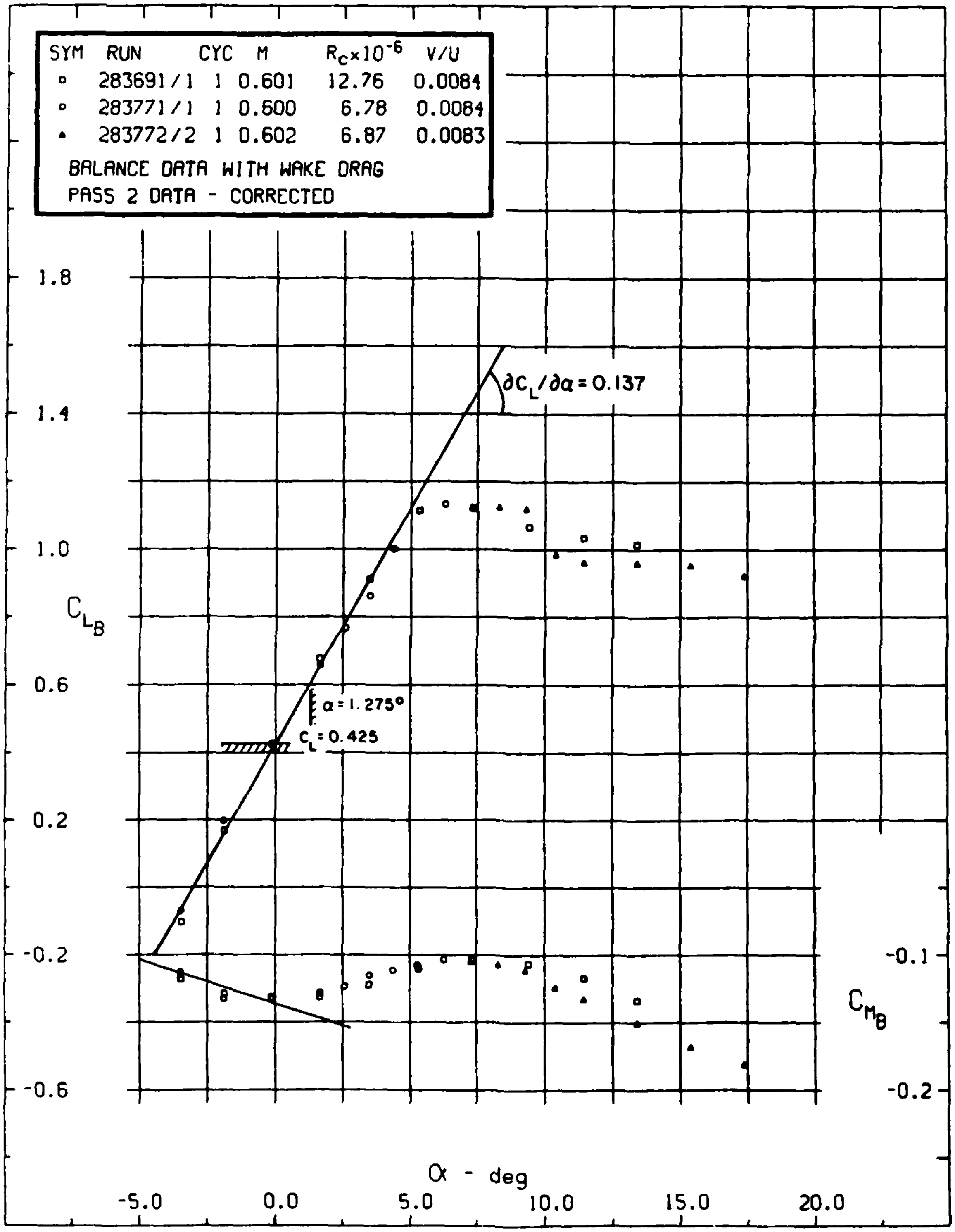

FIG. 4: C_L AND C_M VERSUS α, $M_\infty = 0.6$, $R_c \simeq 6.8$ AND 12.8×10^6

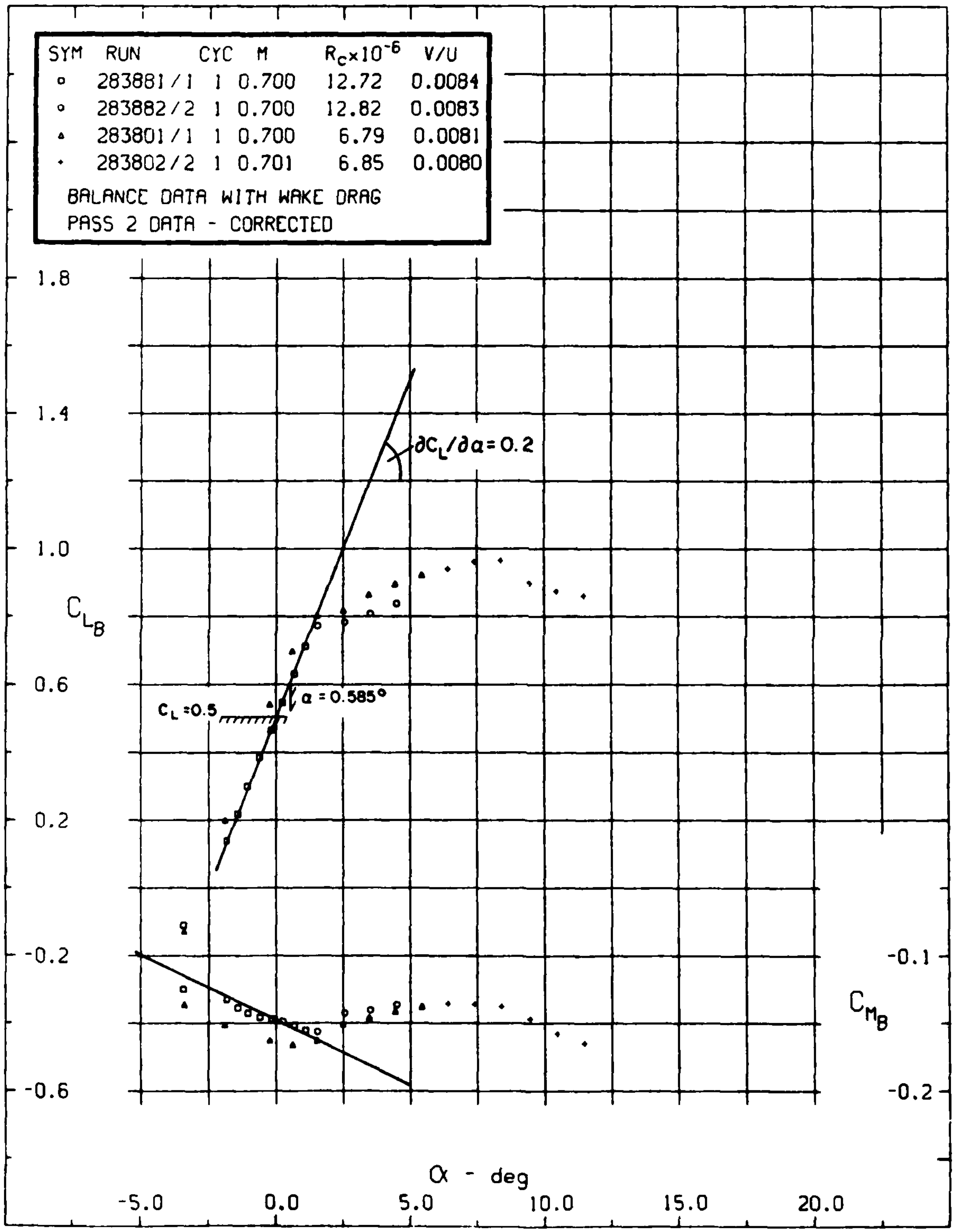

FIG. 5: C_L AND C_M VERSUS α, $M_\infty = 0.3$, $R_c \simeq 6.8$ AND 12.8×10^6

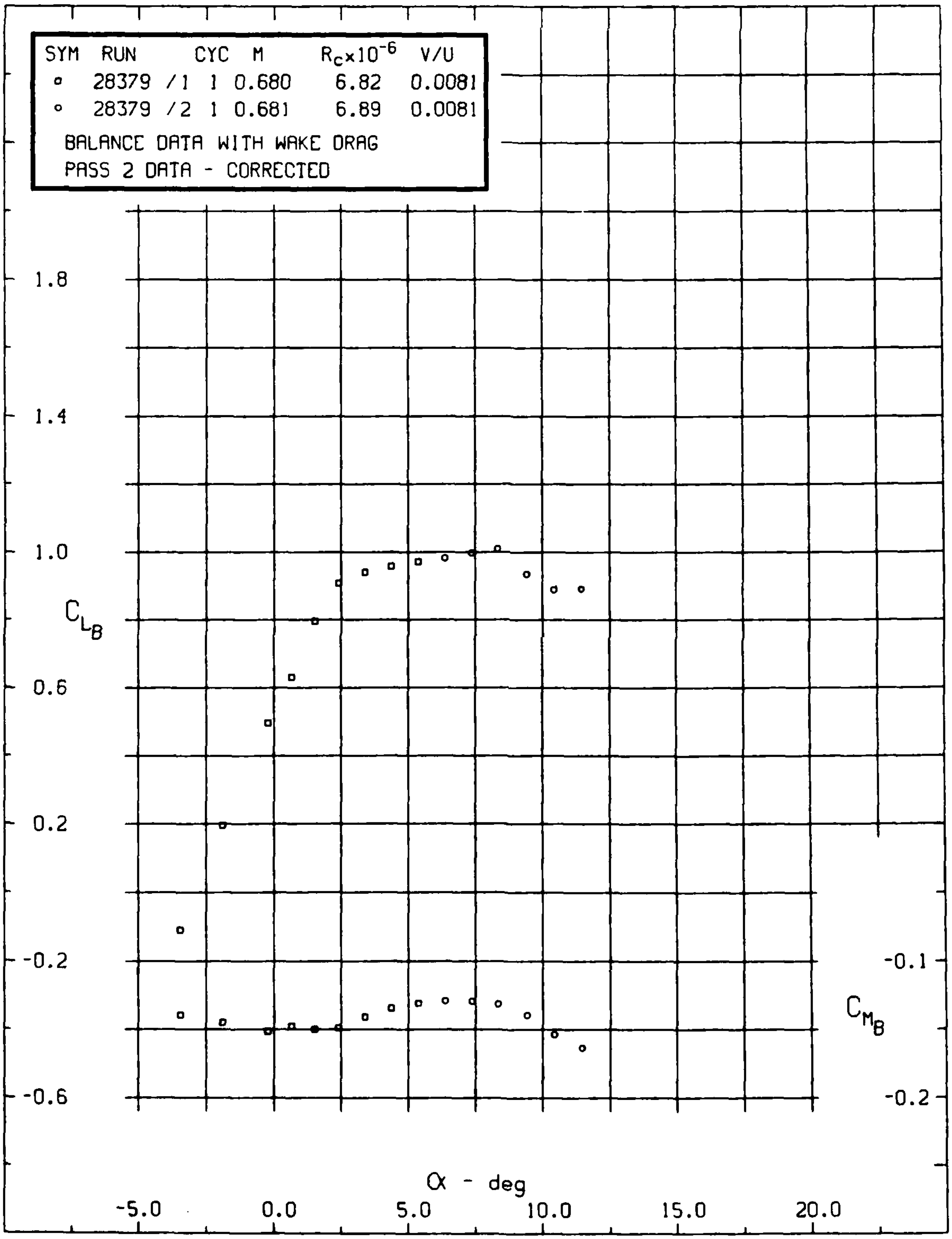

FIG. 6: C_L AND C_M VERSUS α, $R_c \simeq 6.8 \times 10^6$, $M_\infty = 0.68$

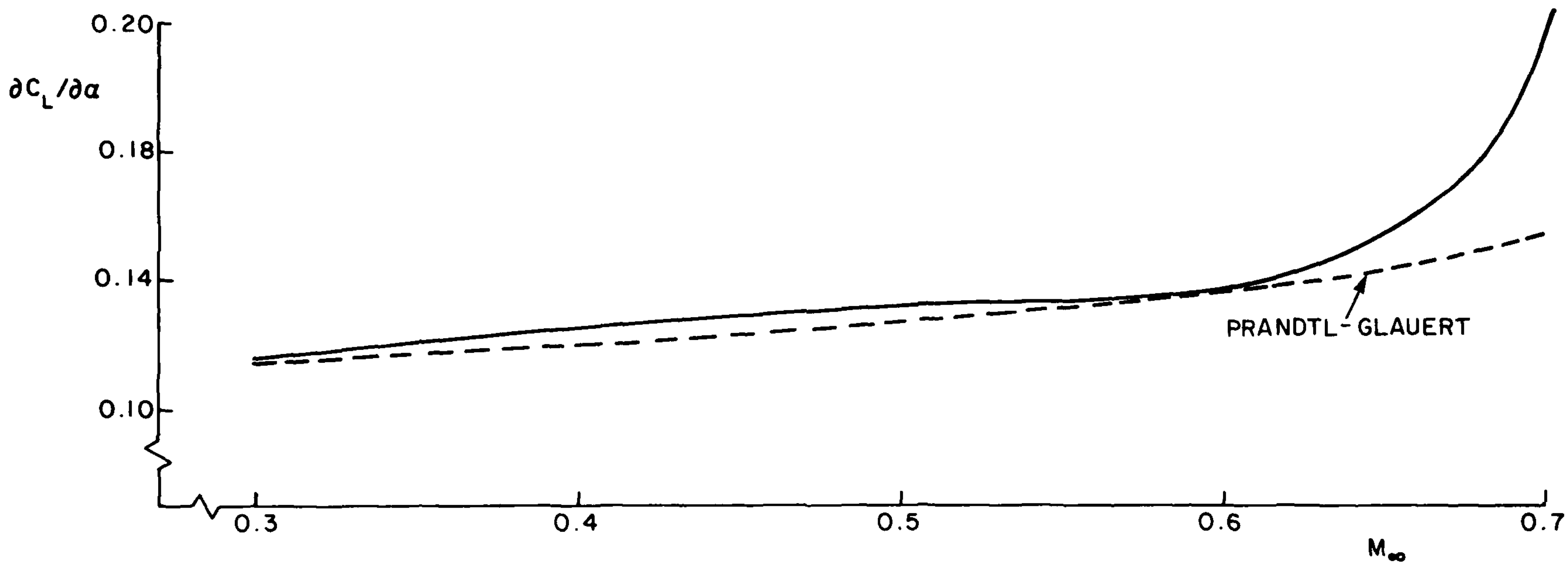

FIG. 7: $\partial C_L/\partial\alpha$ VERSUS FREE STREAM MACH NUMBER (IDENTICAL FOR R_c = 6.8 AND 12.8 $\times$ 10^6)

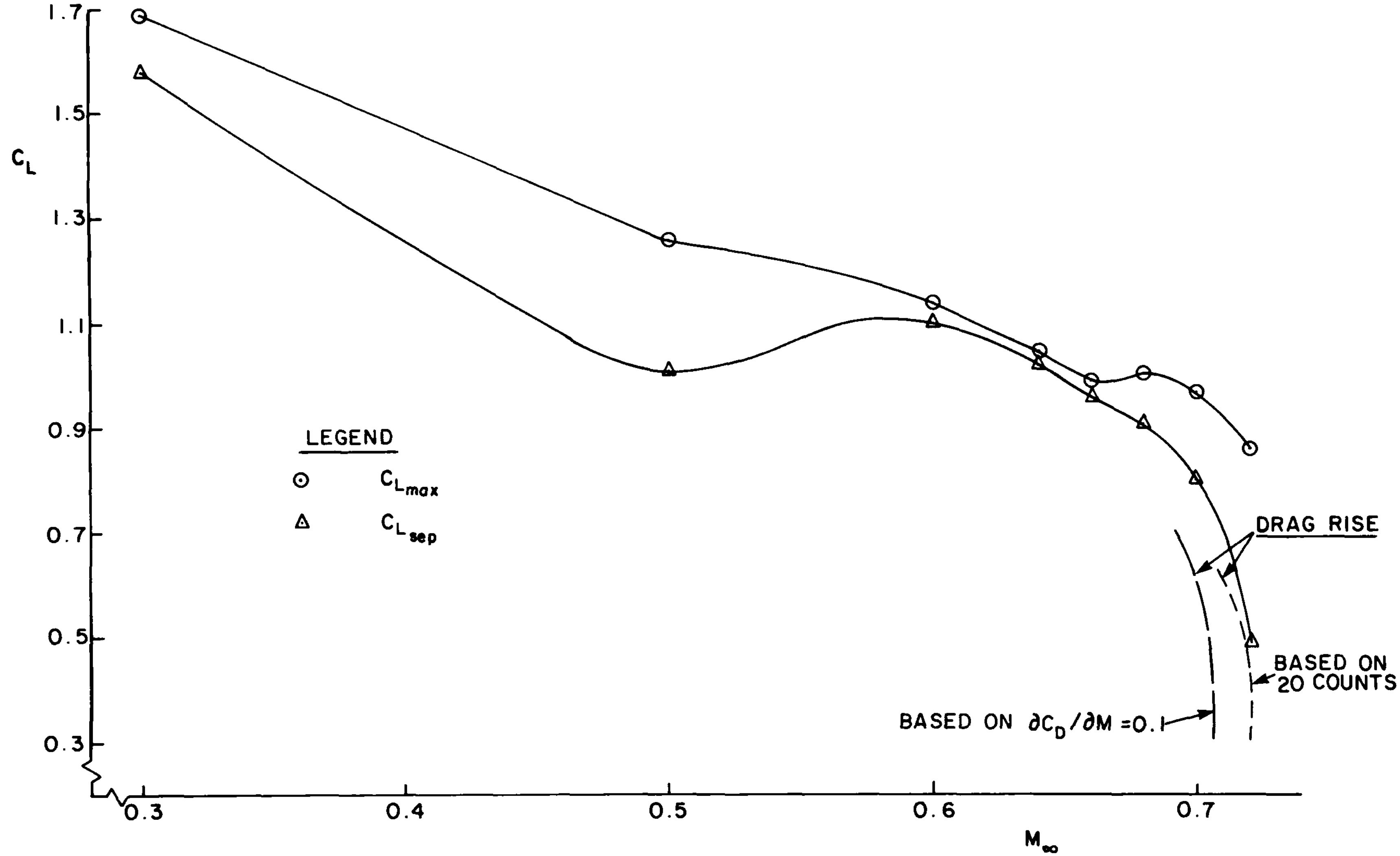

FIG. 8: LIFT PERFORMANCE AT $R_c = 6.8 \times 10^6$

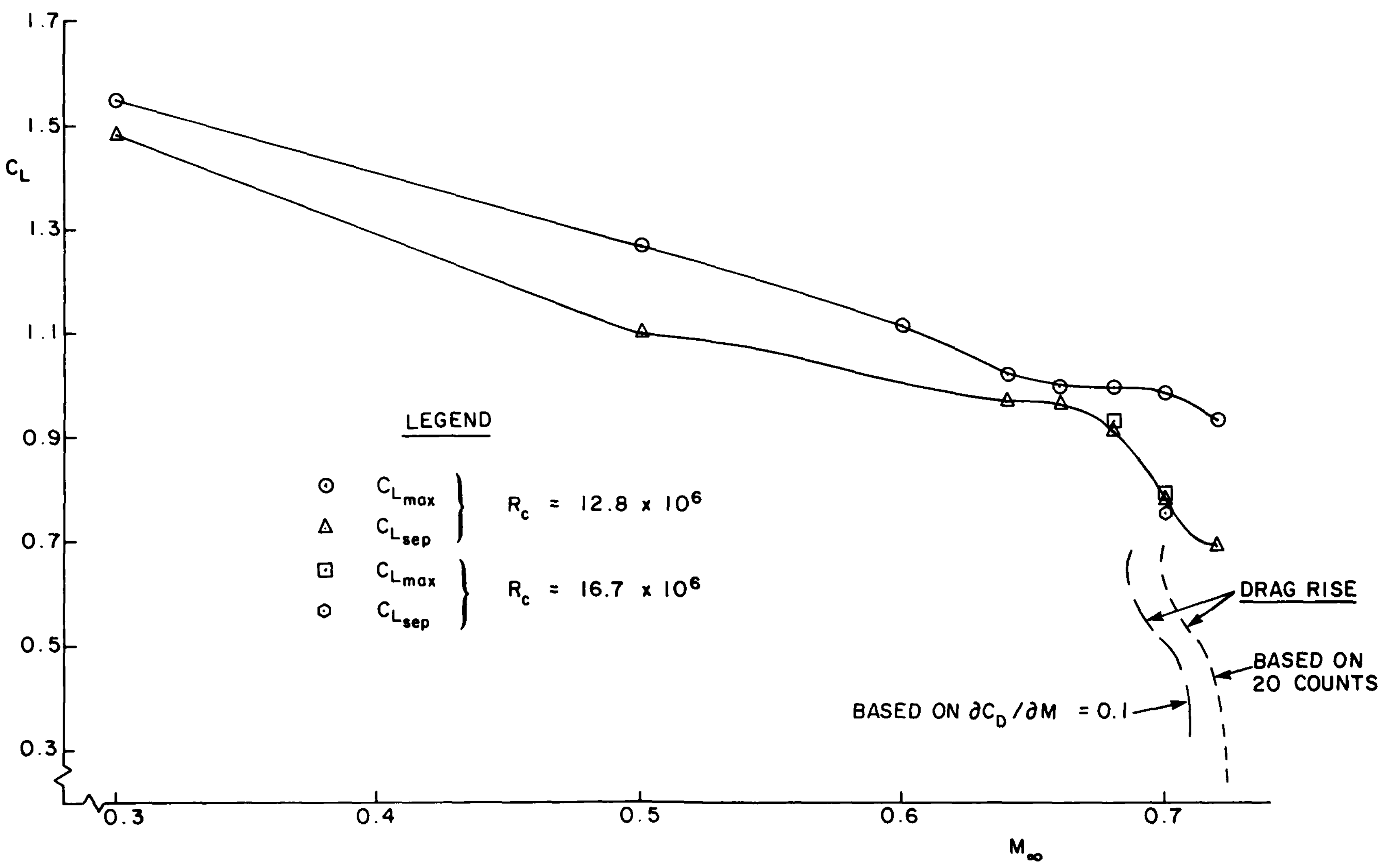

FIG. 9: LIFT PERFORMANCE AT R_c = 12.8 AND 16.7 $\times 10^6$

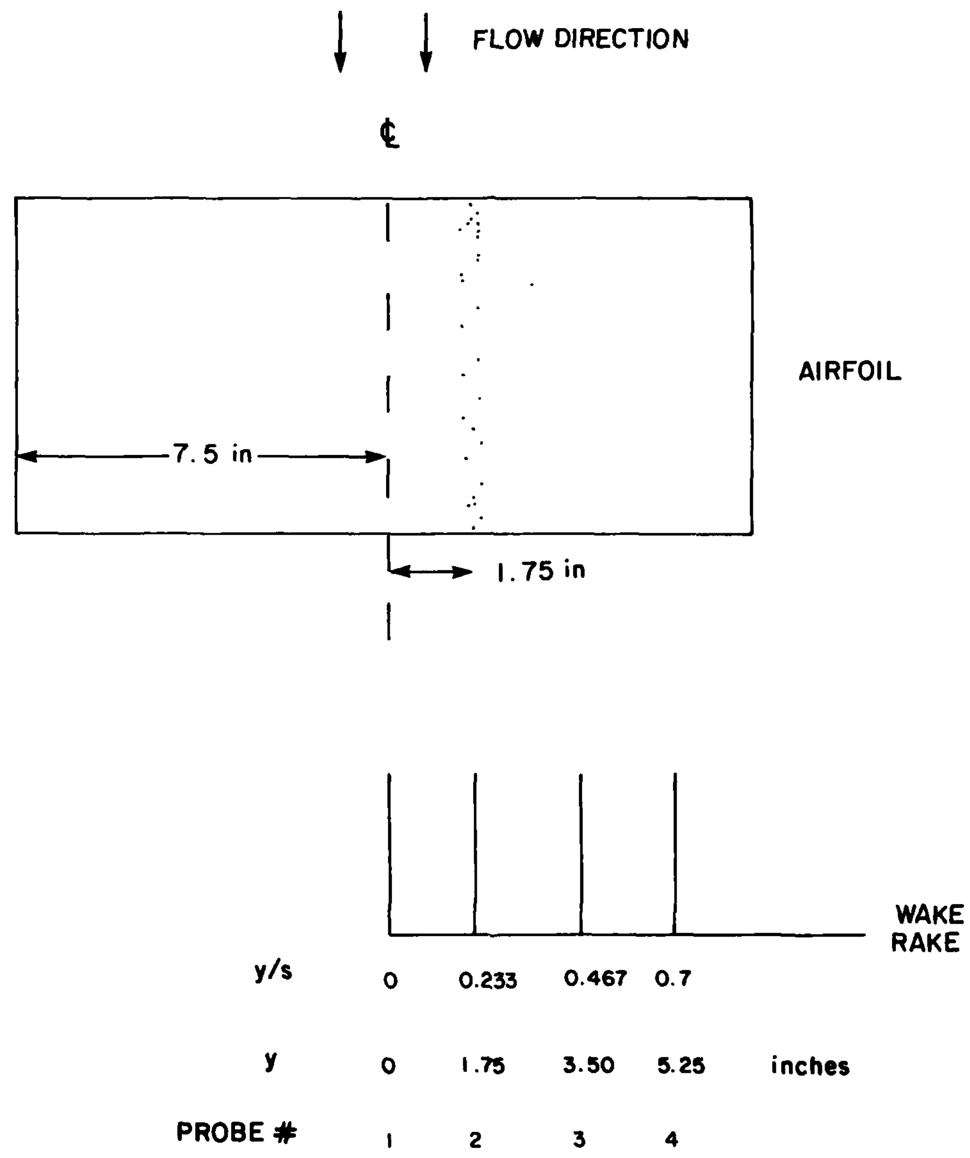

FIG. 10: THE WAKE RAKE PROBE LOCATIONS RELATIVE TO THE AIRFOIL

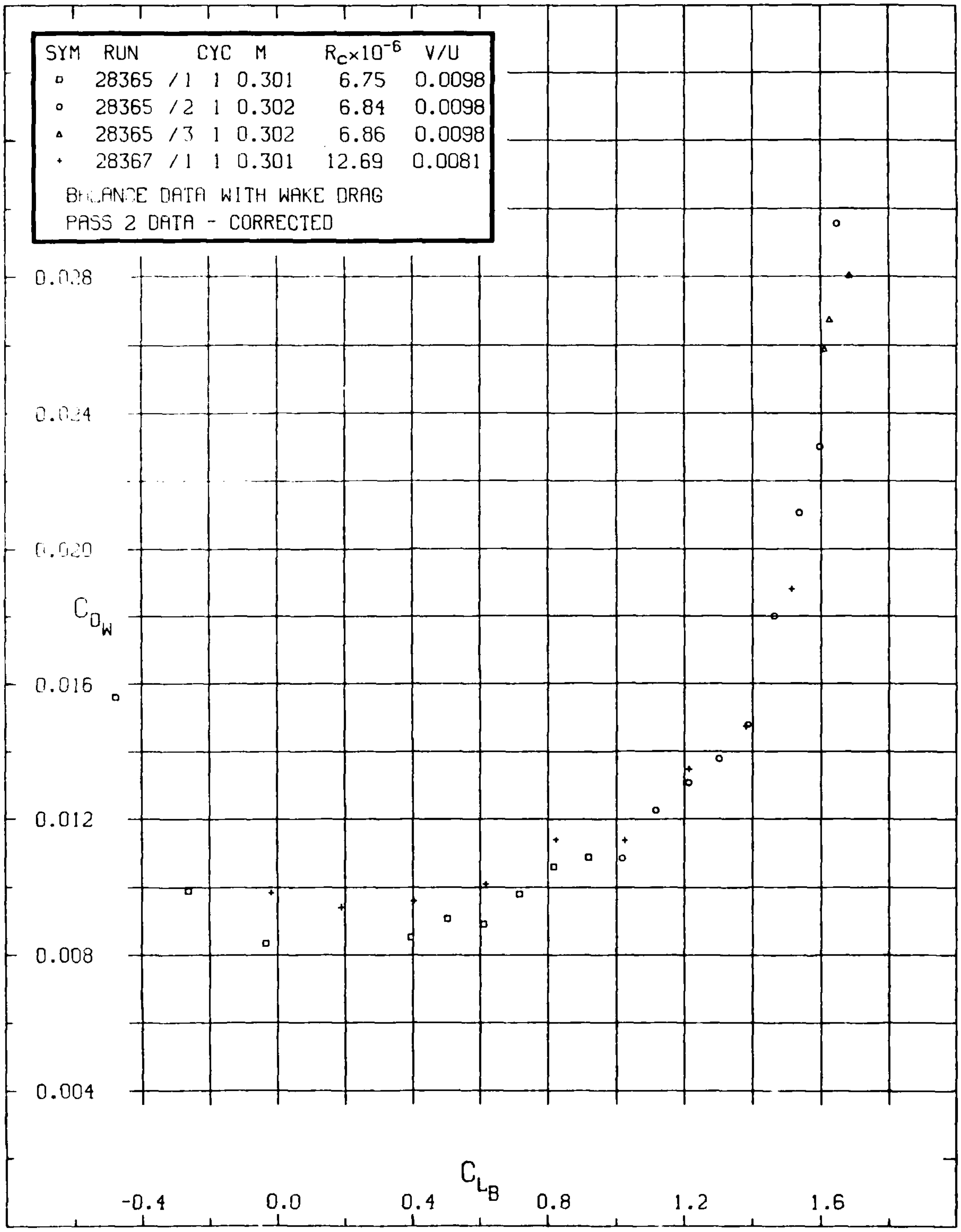

FIG. 11a: C_{D_W} VERSUS C_{L_B} FOR $M_\infty = 0.3$

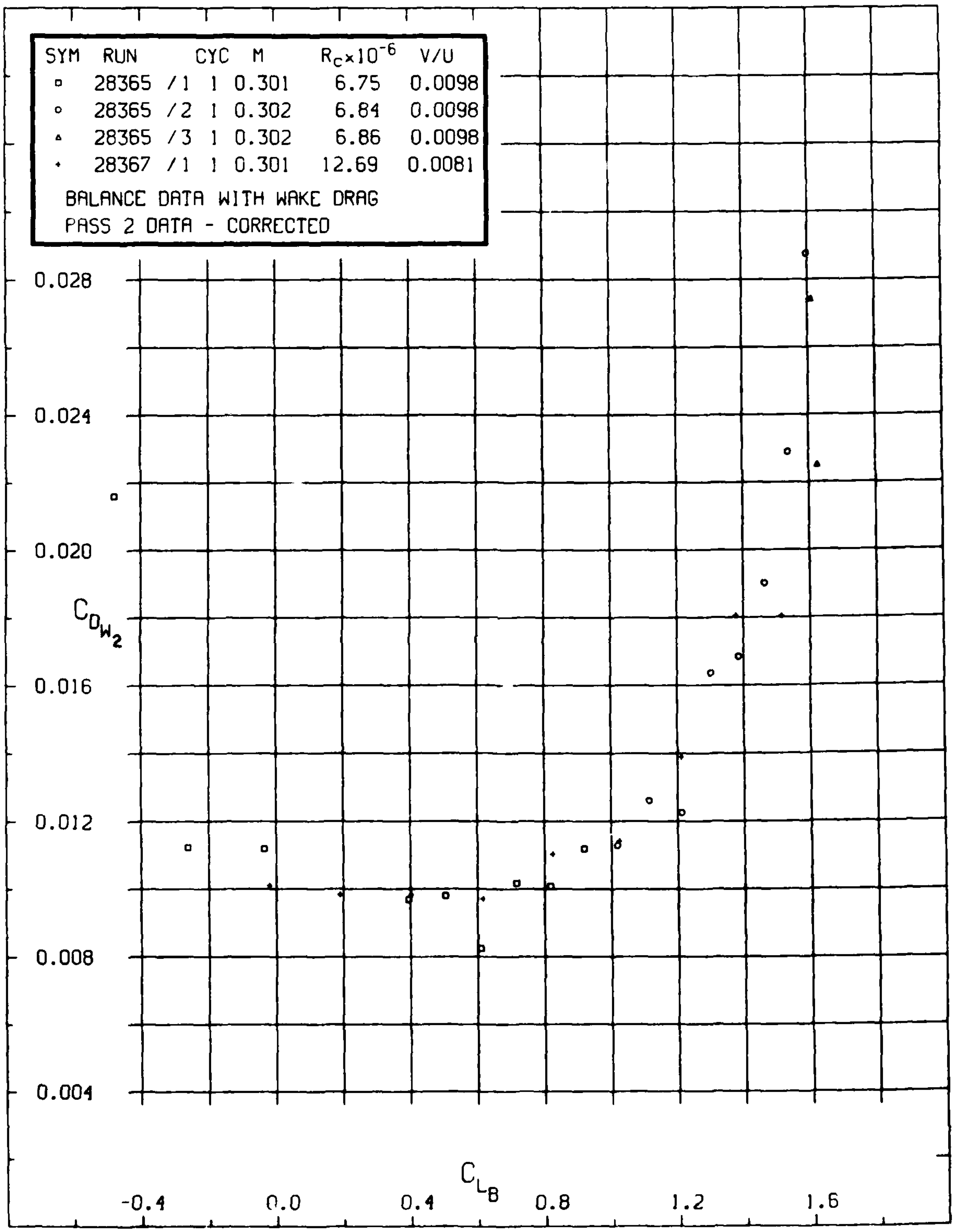

FIG. 11b: $C_{D_{W_2}}$ VERSUS C_{L_B} FOR $M_\infty = 0.3$

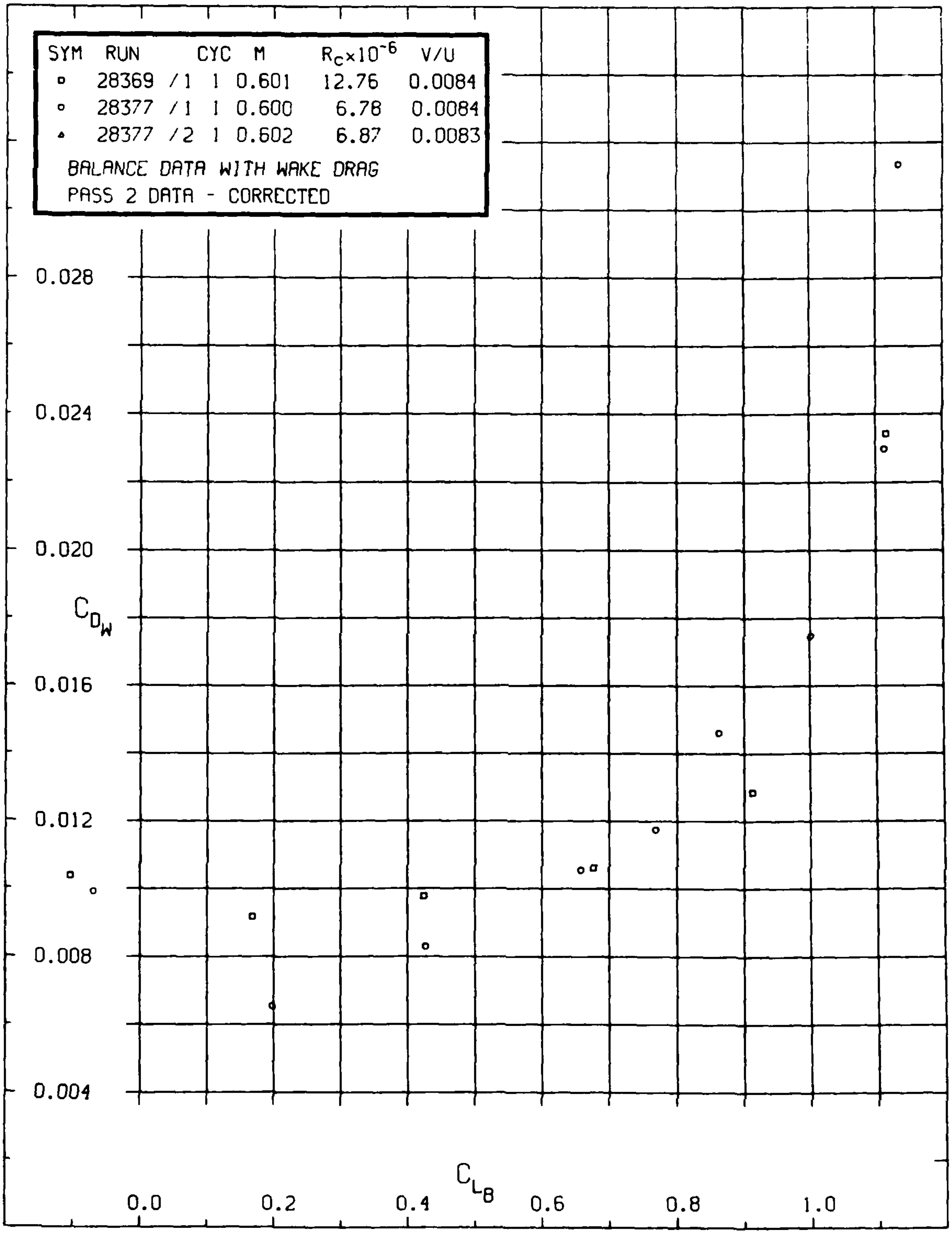

FIG. 12a: C_{D_W} VERSUS C_{L_B} FOR $M_\infty = 0.6$

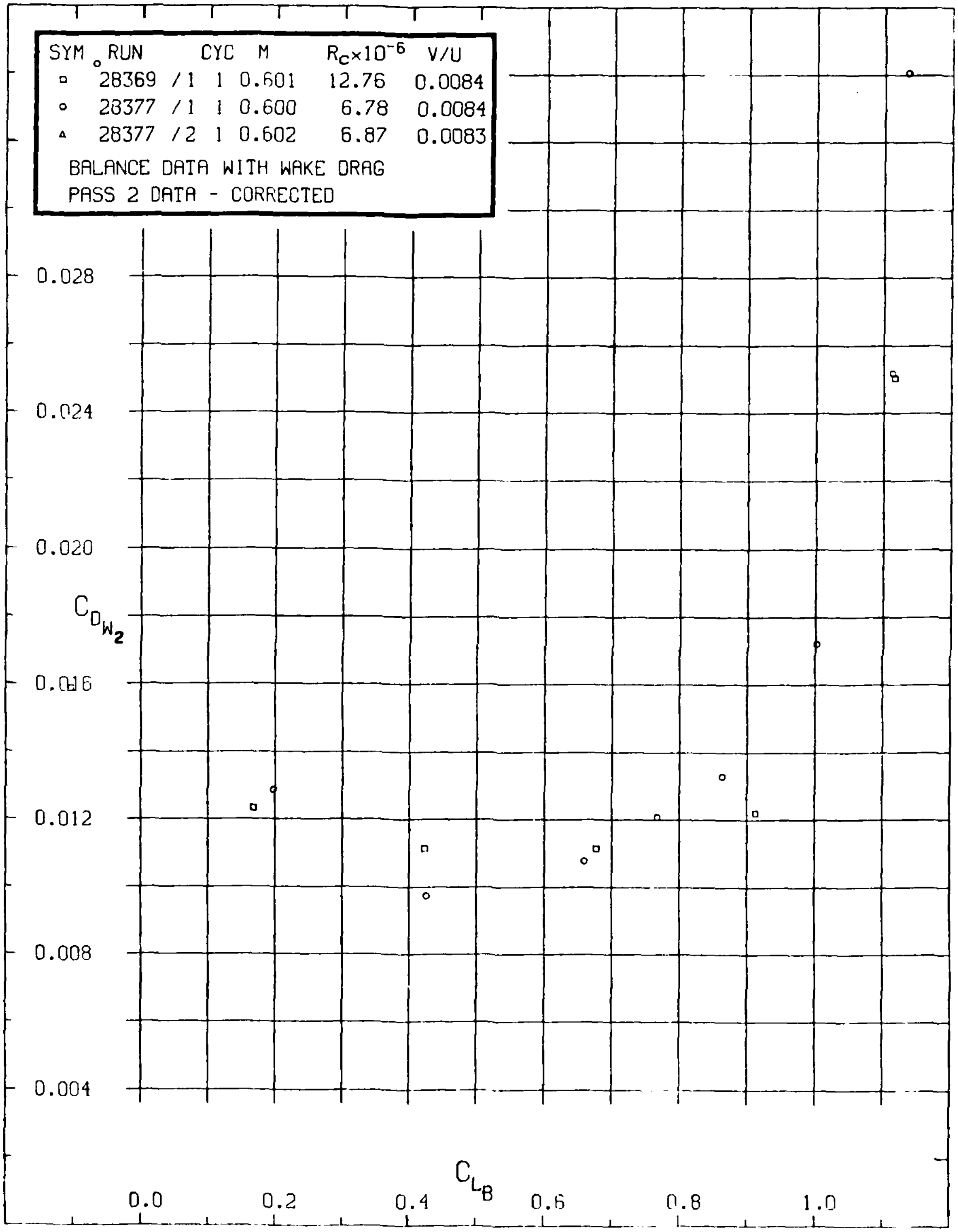

FIG. 12b: $C_{D_{W_2}}$ VERSUS C_{L_B} FOR $M_\infty = 0.6$

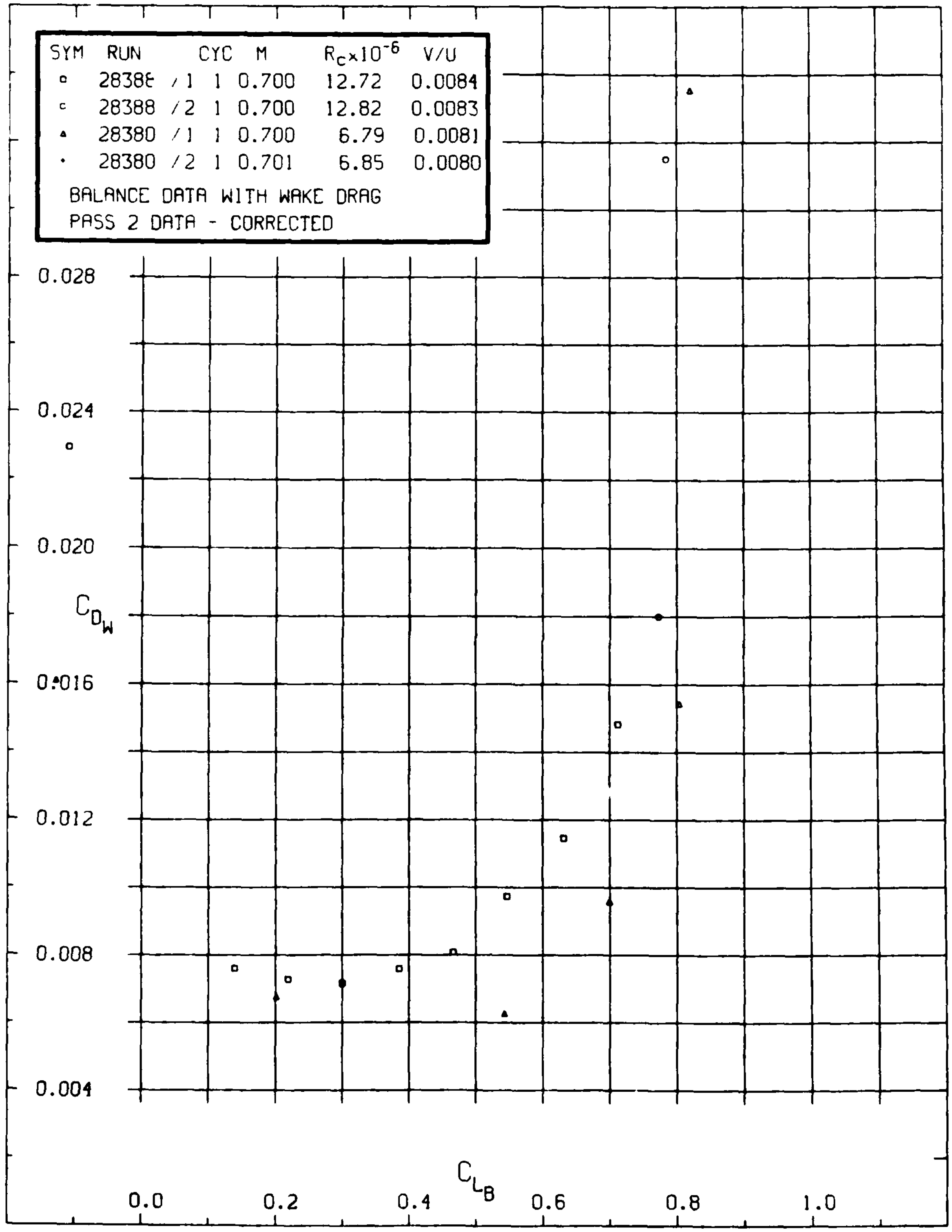

FIG. 13a: C_{D_W} VERSUS C_{L_B} FOR $M_\infty = 0.7$

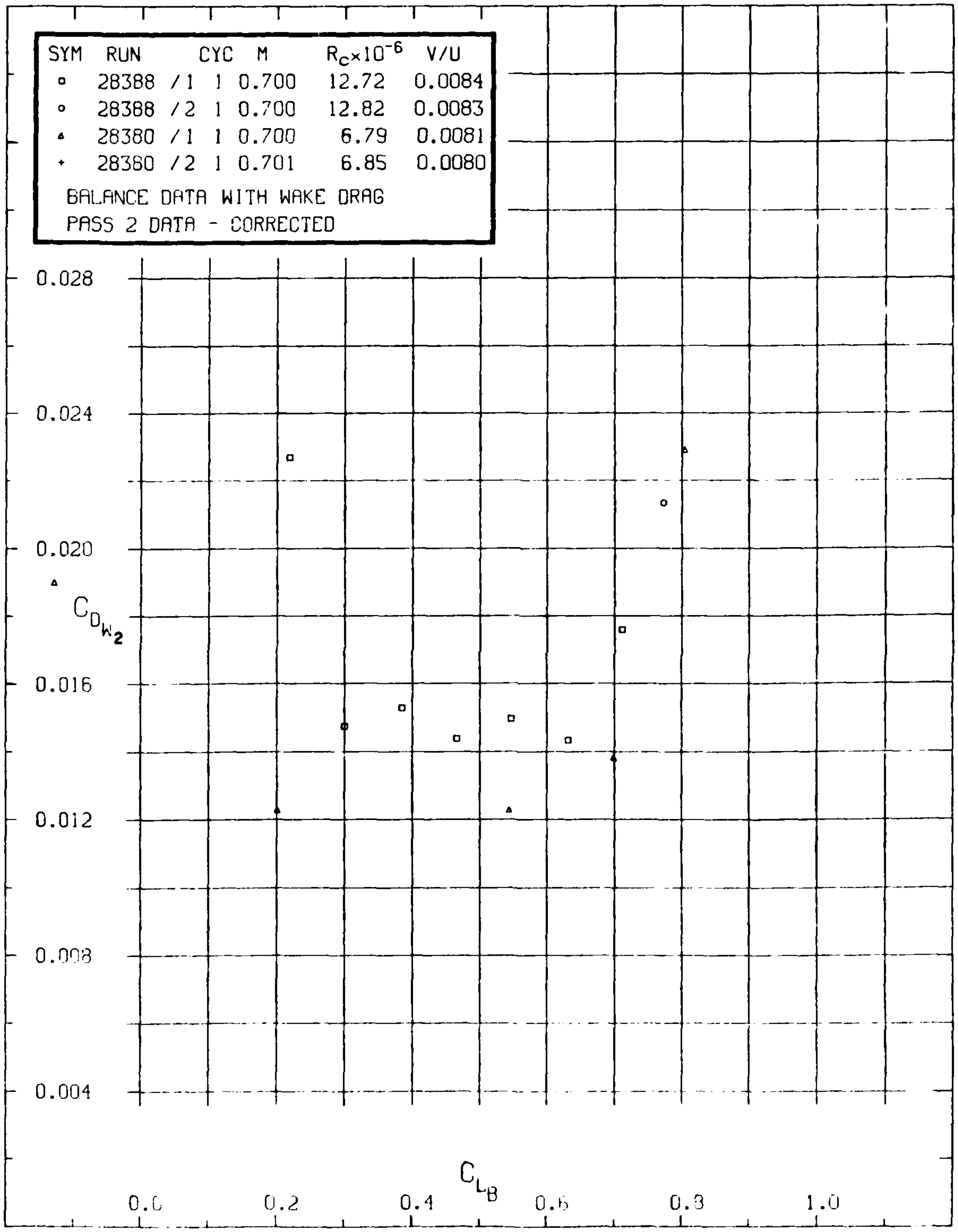

FIG. 13b: $C_{D_{W_2}}$ VERSUS C_{L_B} FOR $M_\infty = 0.7$

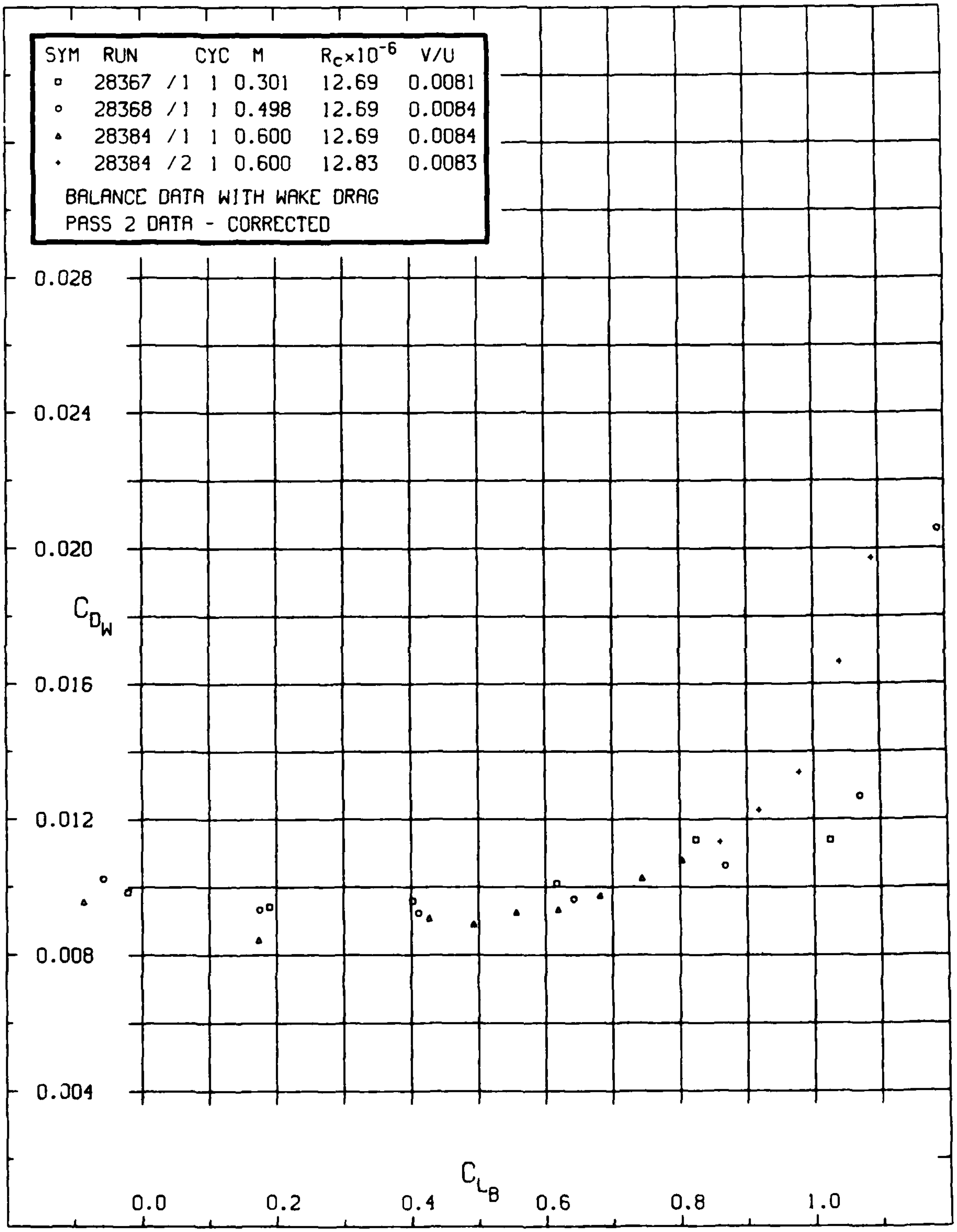

FIG. 14a: C_{D_W} VERSUS C_{L_B} FOR M_∞ = 0.3, 0.5 AND 0.6

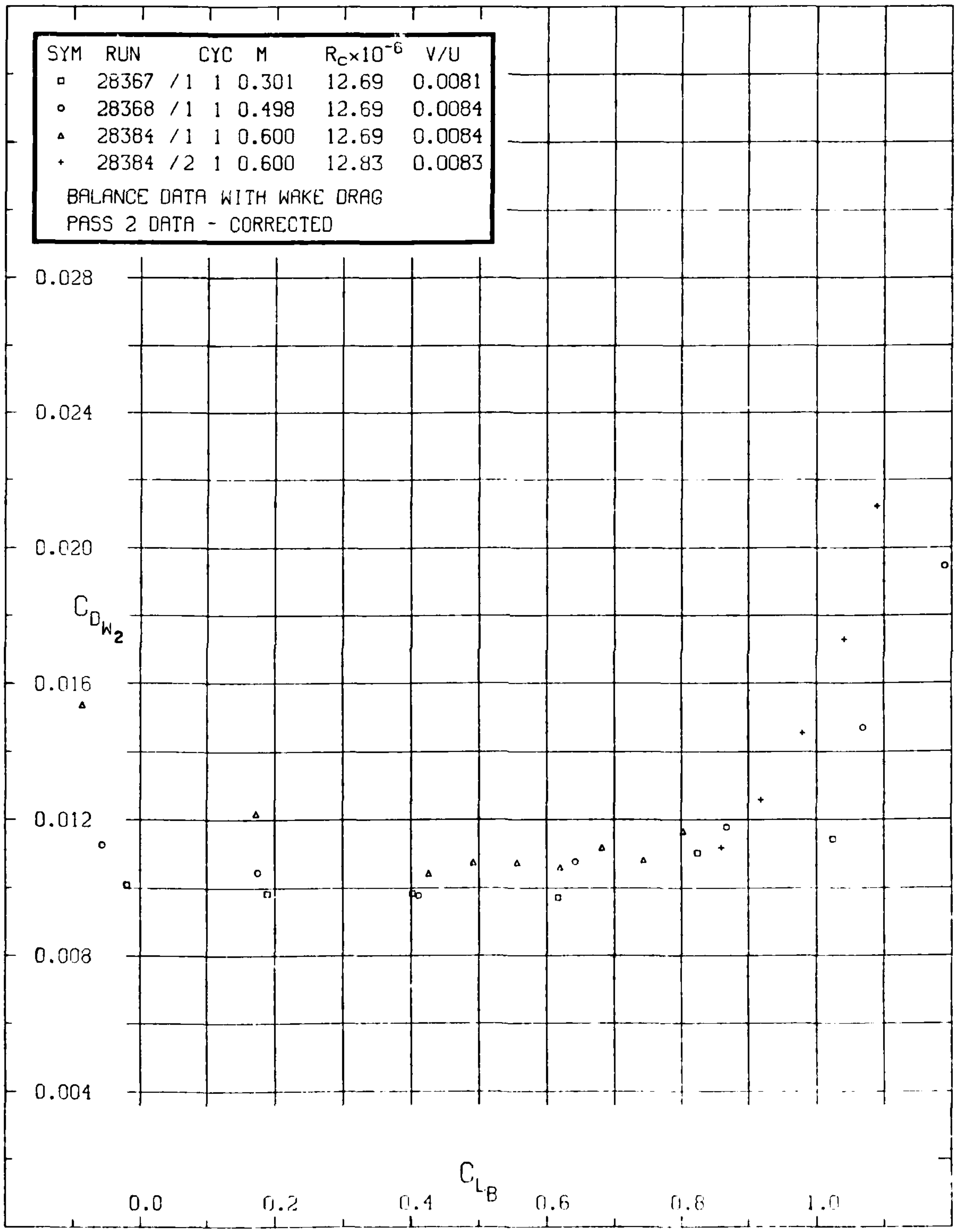

FIG. 14b: $C_{D_{W_2}}$ VERSUS C_{L_B} FOR M_∞ = 0.3, 0.5 AND 0.6

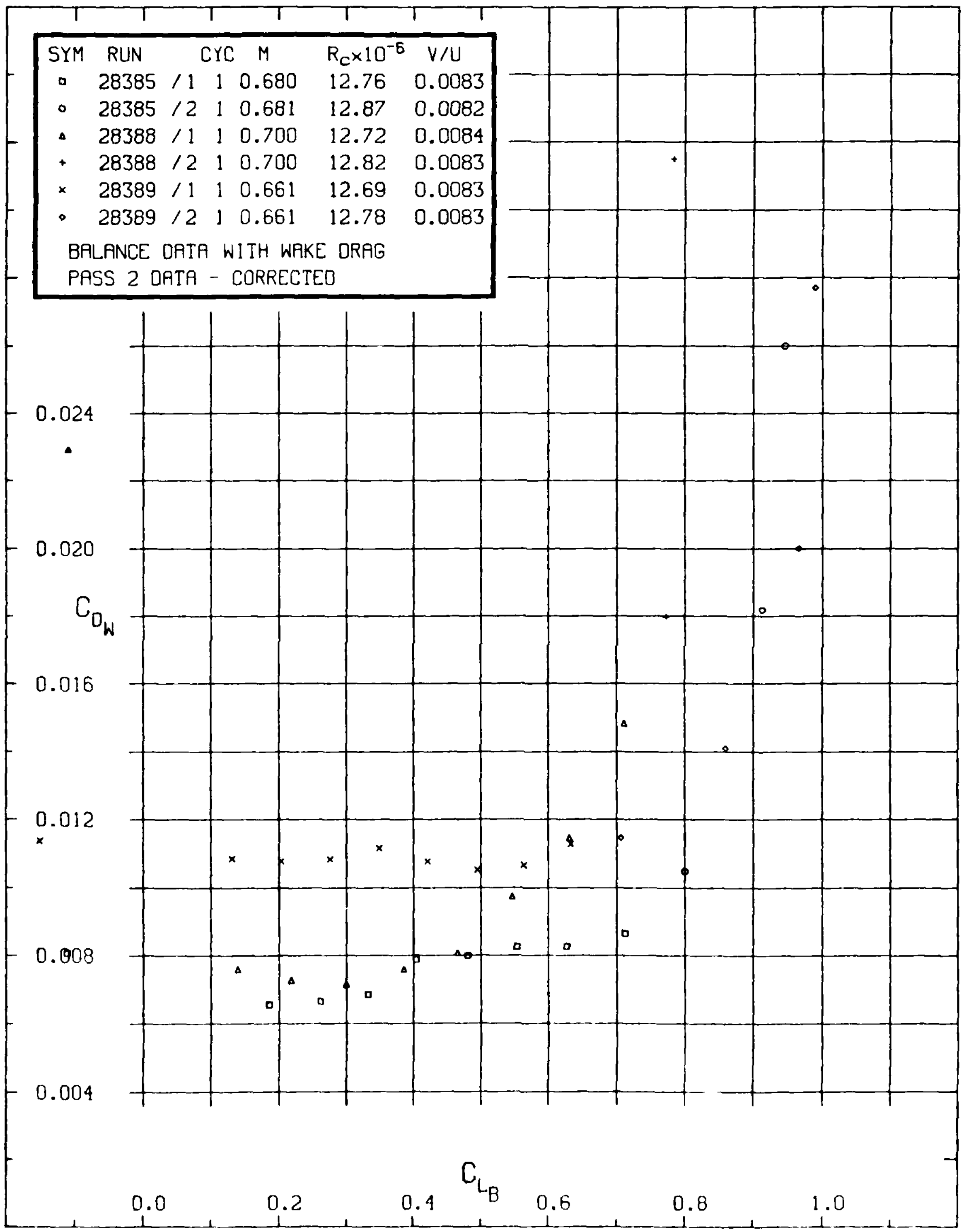

FIG. 15a: C_{D_W} VERSUS C_{L_B} FOR $M_\infty = 0.66, 0.68$ AND 0.70

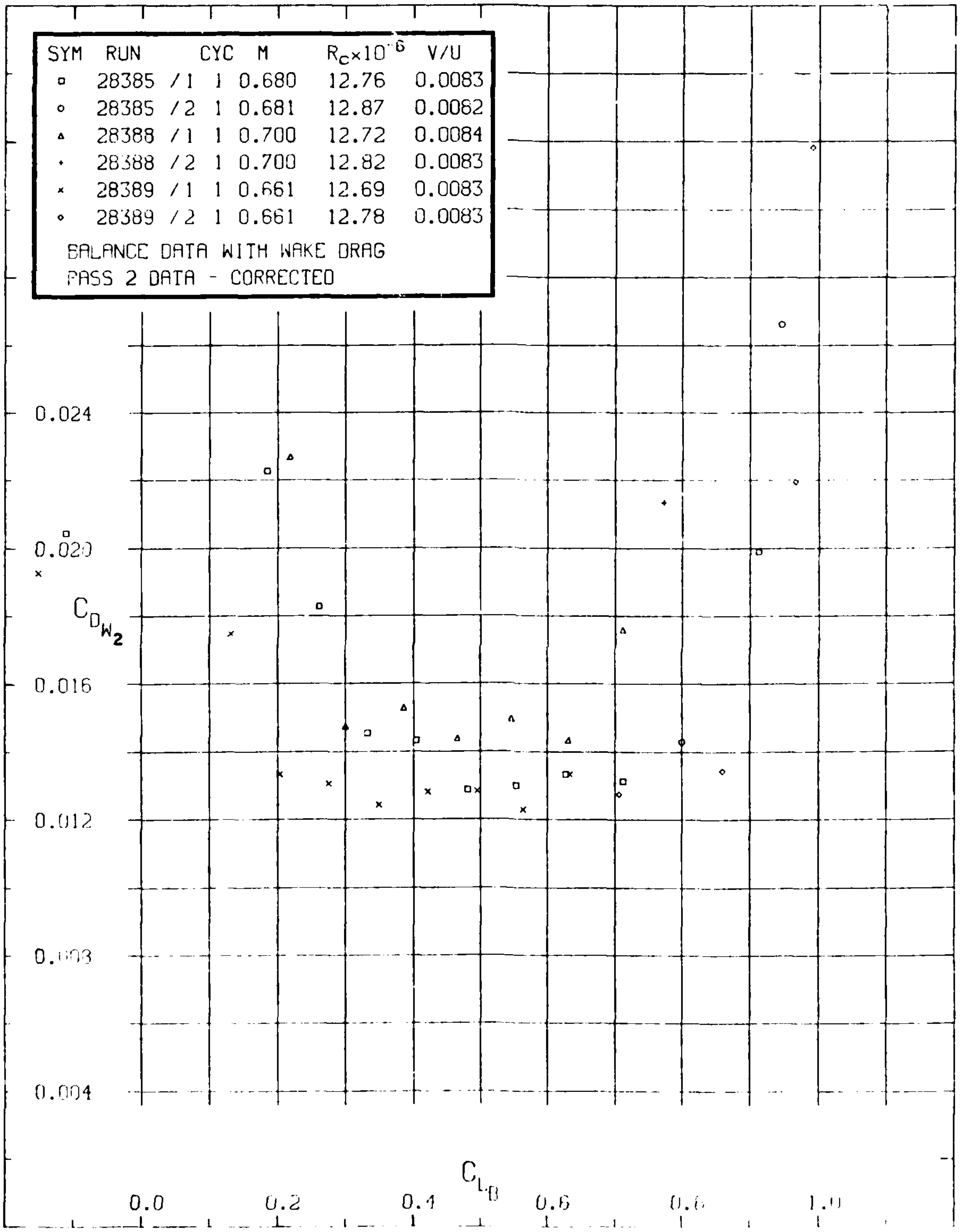

FIG. 15b: $C_{D_{W_2}}$ VERSUS C_{L_B} FOR M_∞ = 0.66, 0.68 AND 0.70

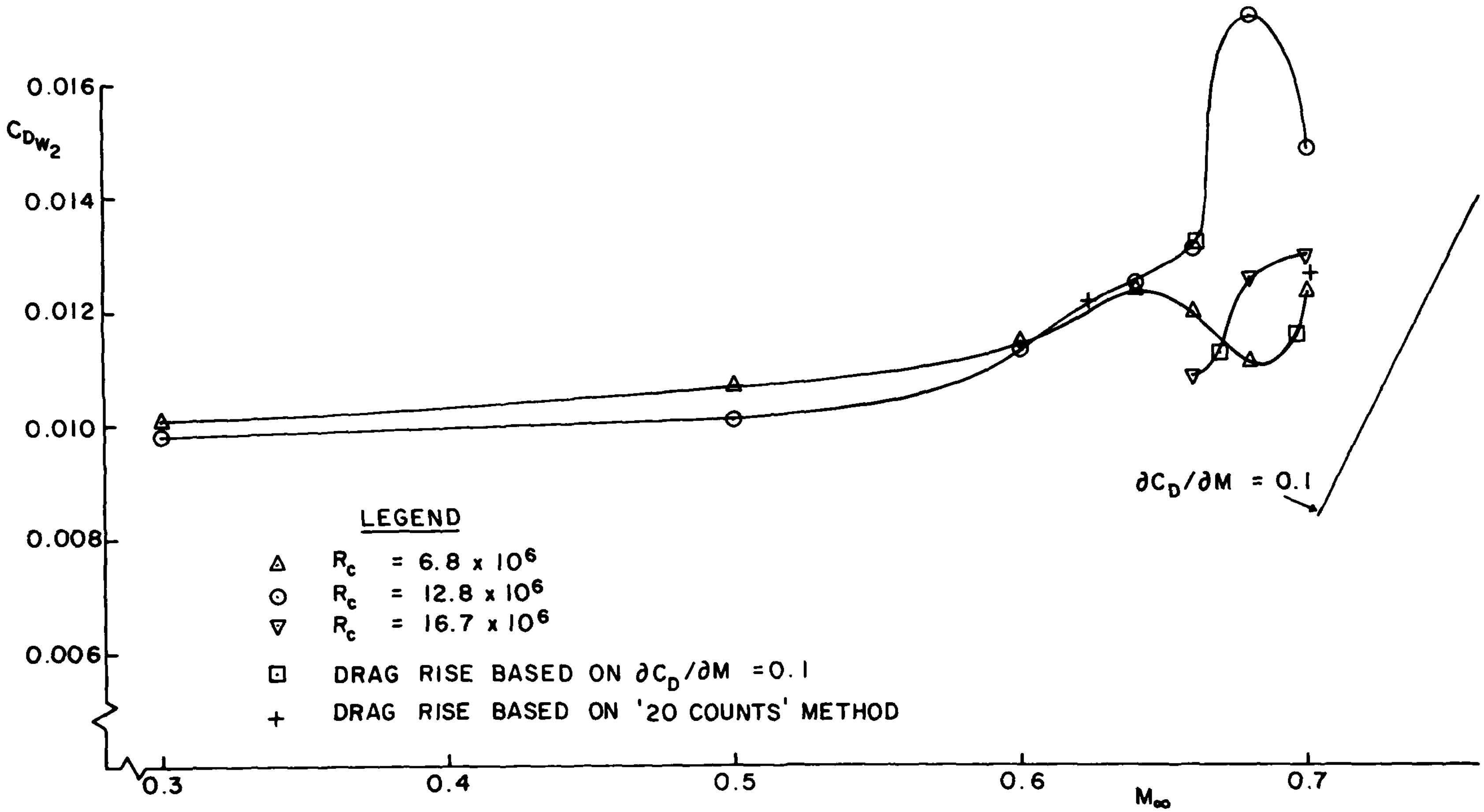

FIG. 16a: $C_{D_{W_2}}$ VERSUS M_∞ FOR $C_L = 0.3$

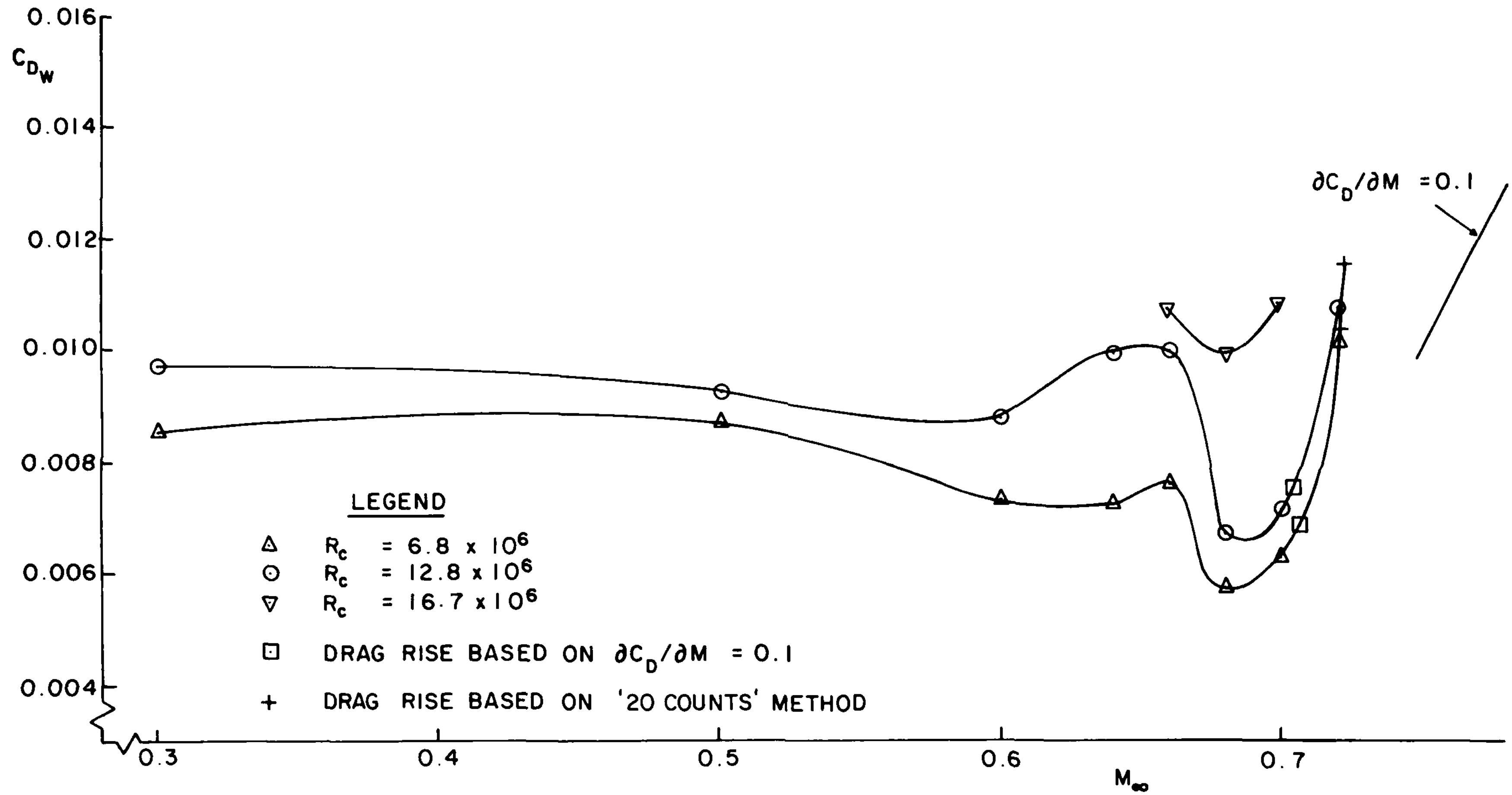

FIG. 16b: C_{D_W} VERSUS M_∞ FOR C_L = 0.3

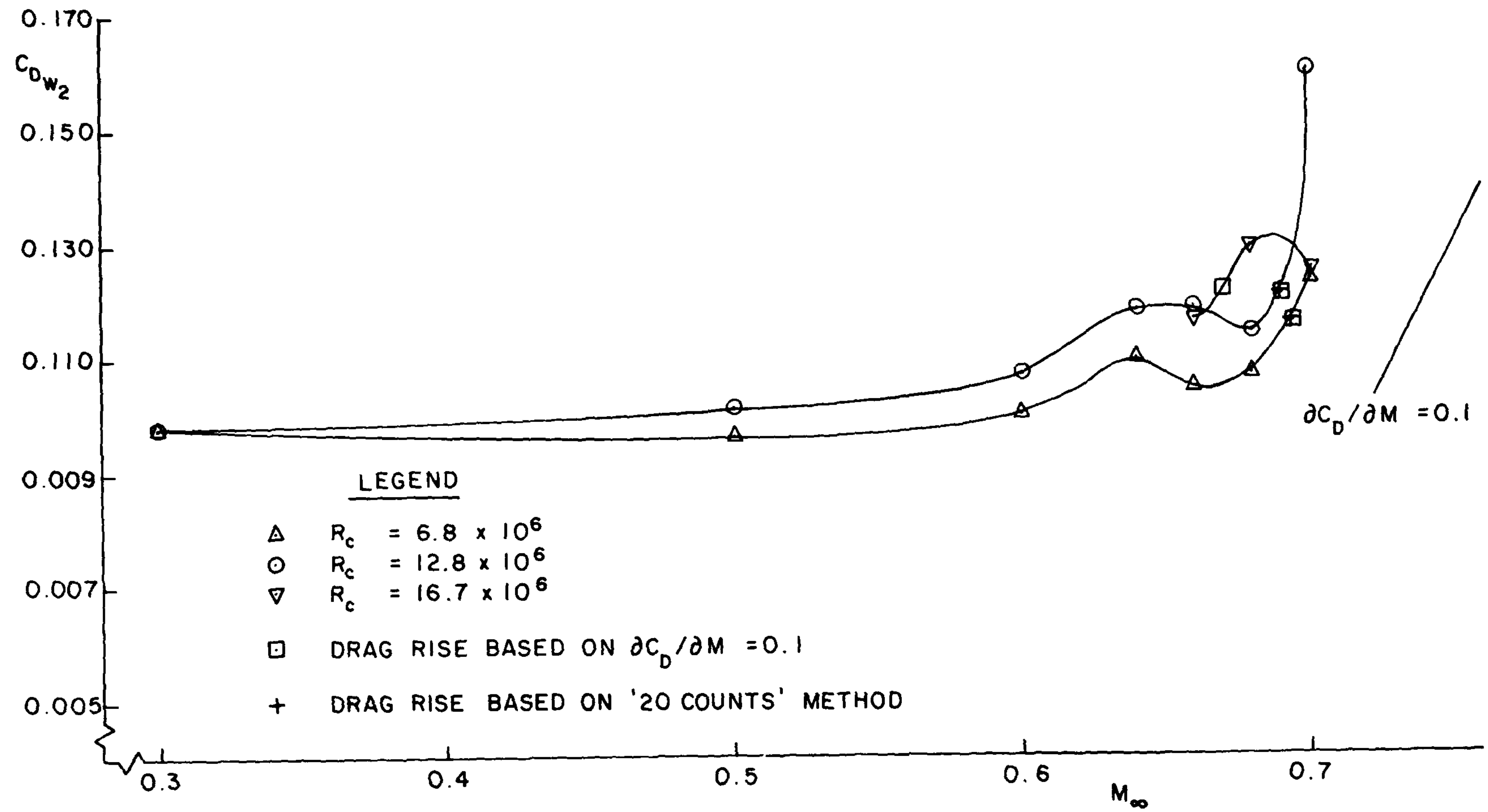

FIG. 17a: $C_{D_{W_2}}$ VERSUS M_∞ FOR $C_L = 0.5$

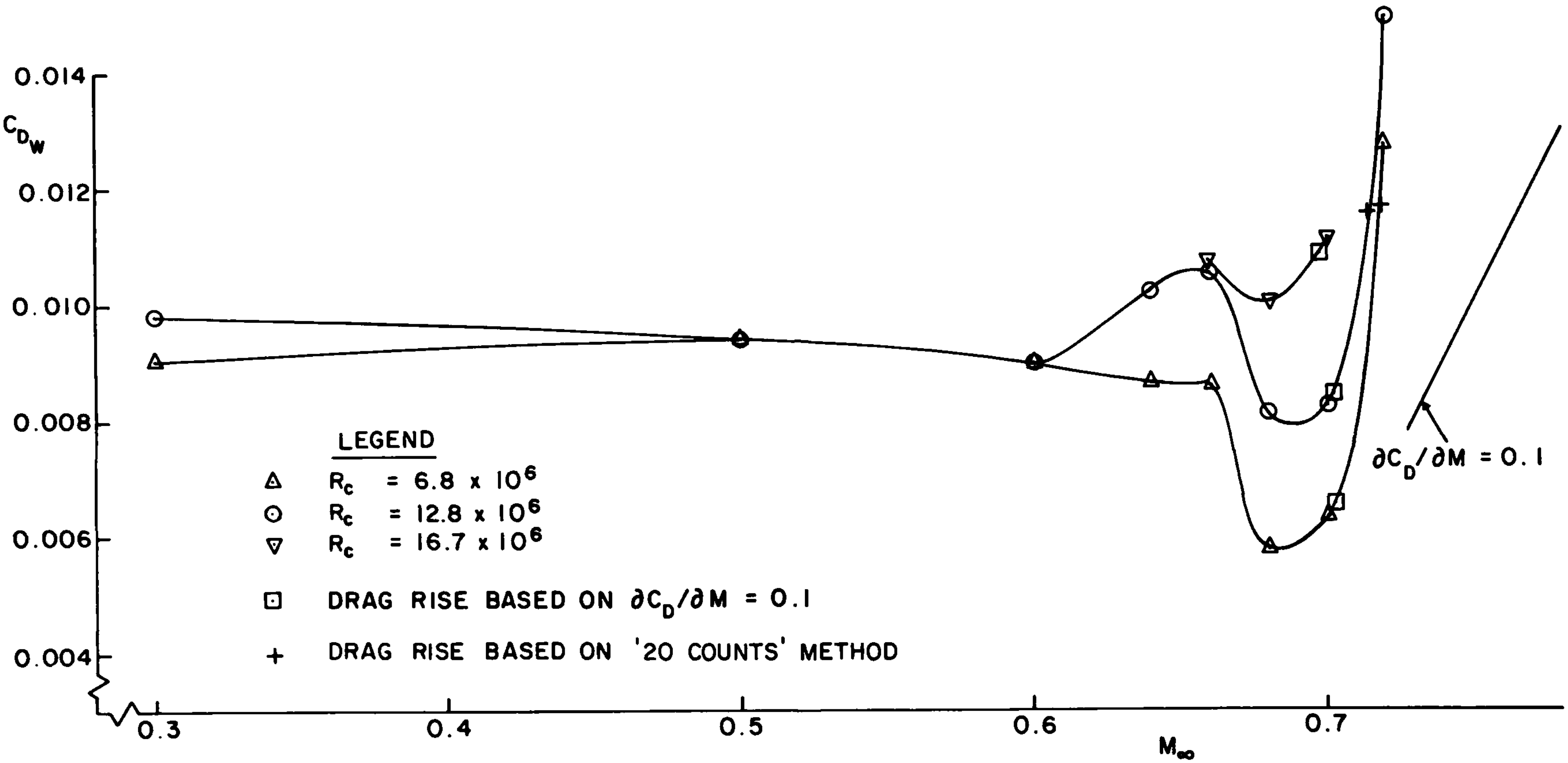

FIG. 17b: C_{D_W} VERSUS M_∞ FOR $C_L = 0.5$

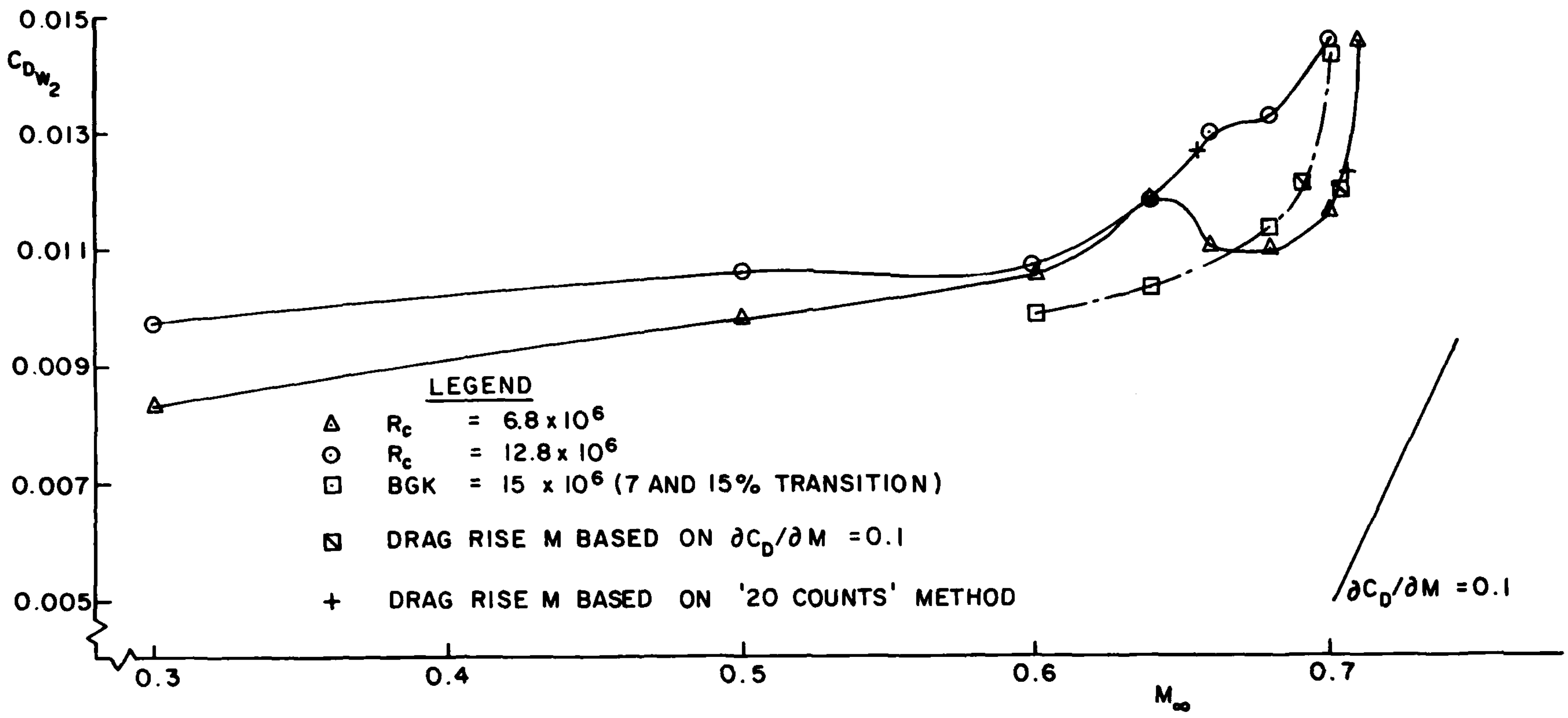

FIG. 18a: $C_{D_{W_2}}$ VERSUS M_∞ FOR C_L = 0.6

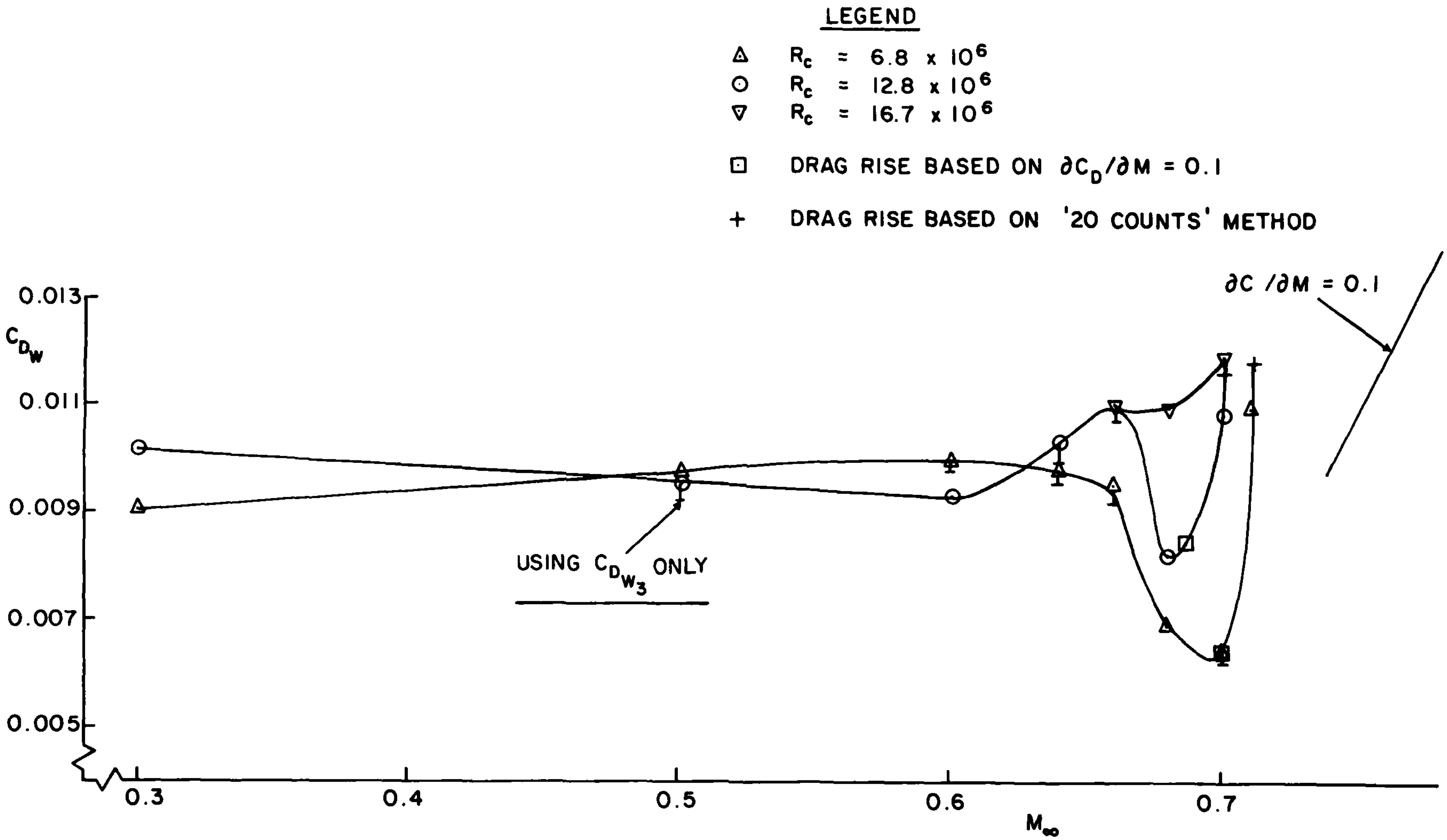

FIG. 18b: C_{D_W} VERSUS M_∞ FOR $C_L = 0.6$

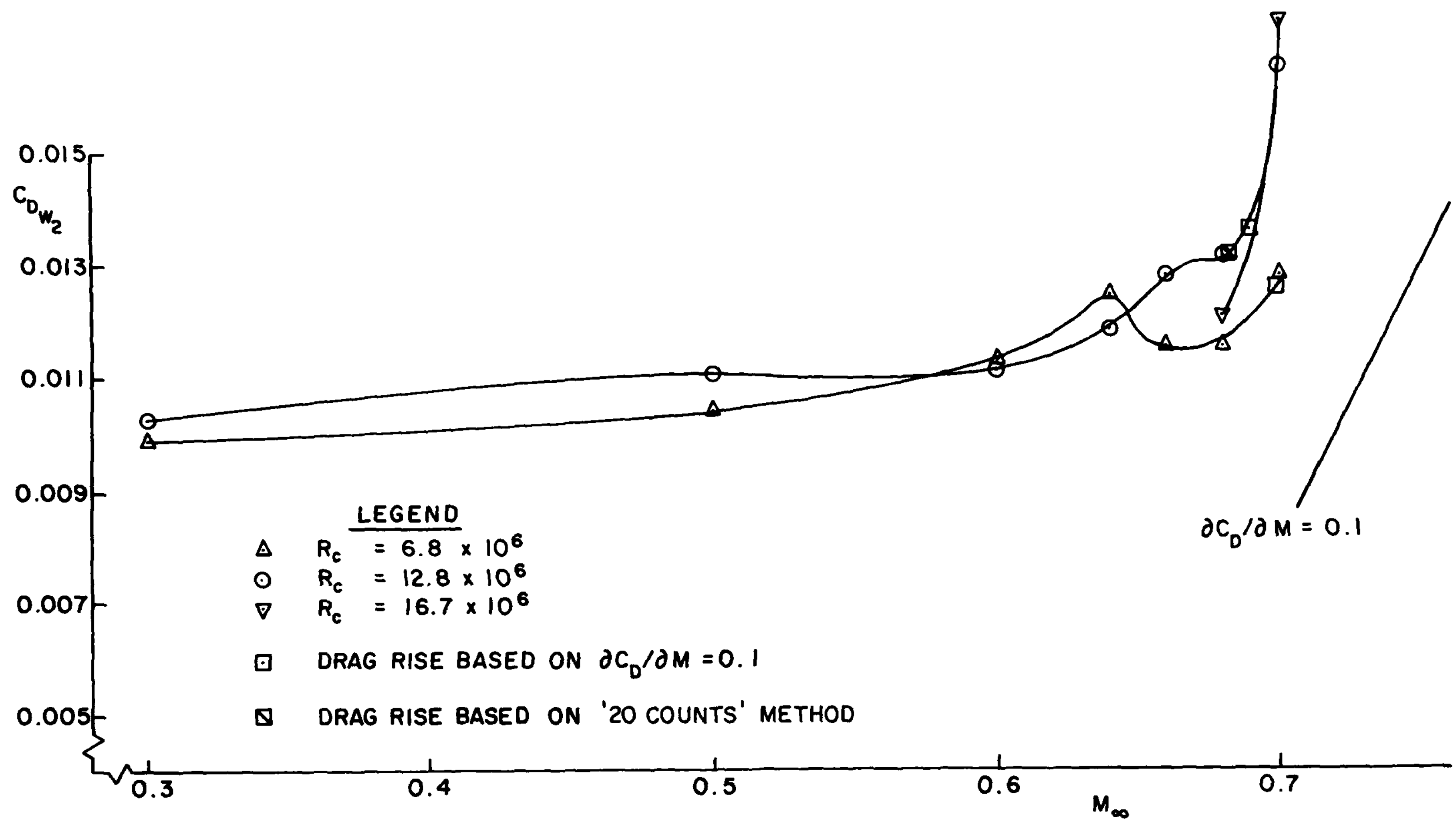

FIG. 19a: $C_{D_{W_2}}$ VERSUS M_∞ FOR $C_L = 0.7$

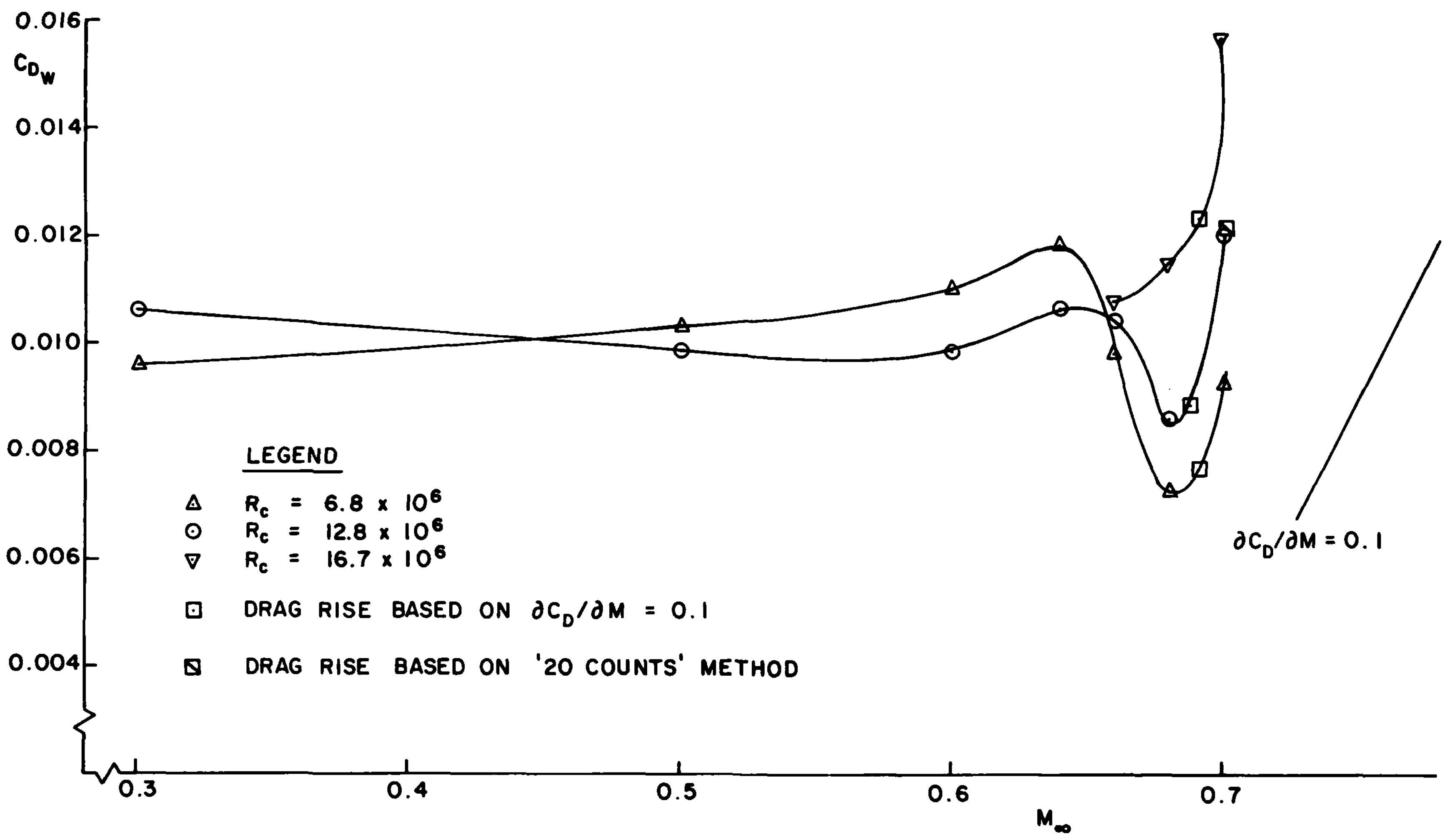

FIG. 19b: C_{D_W} VERSUS M_∞ FOR $C_L = 0.7$

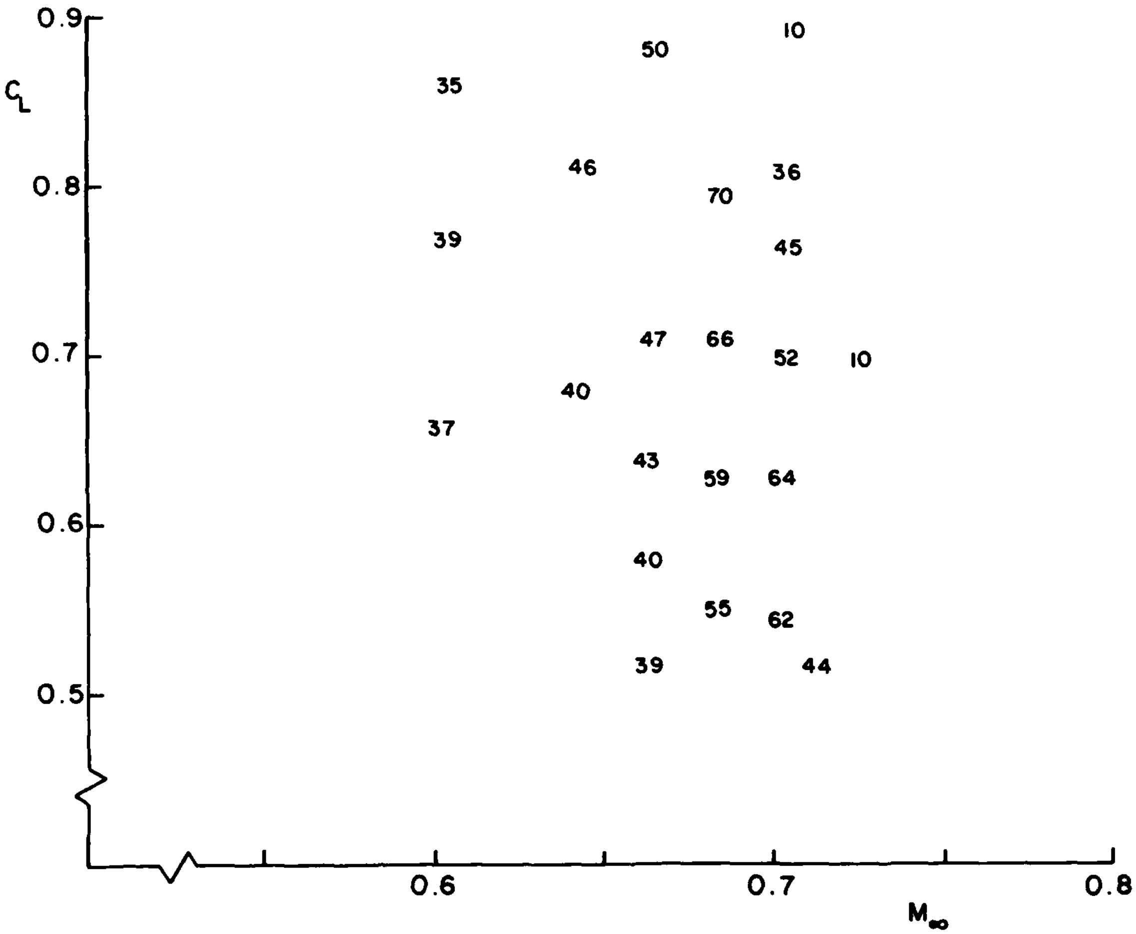

FIG. 20a: RANGE PARAMETER $M_\infty C_L / C_{DW}$ VALUES FOR $R_c = 6.8 \times 10^6$

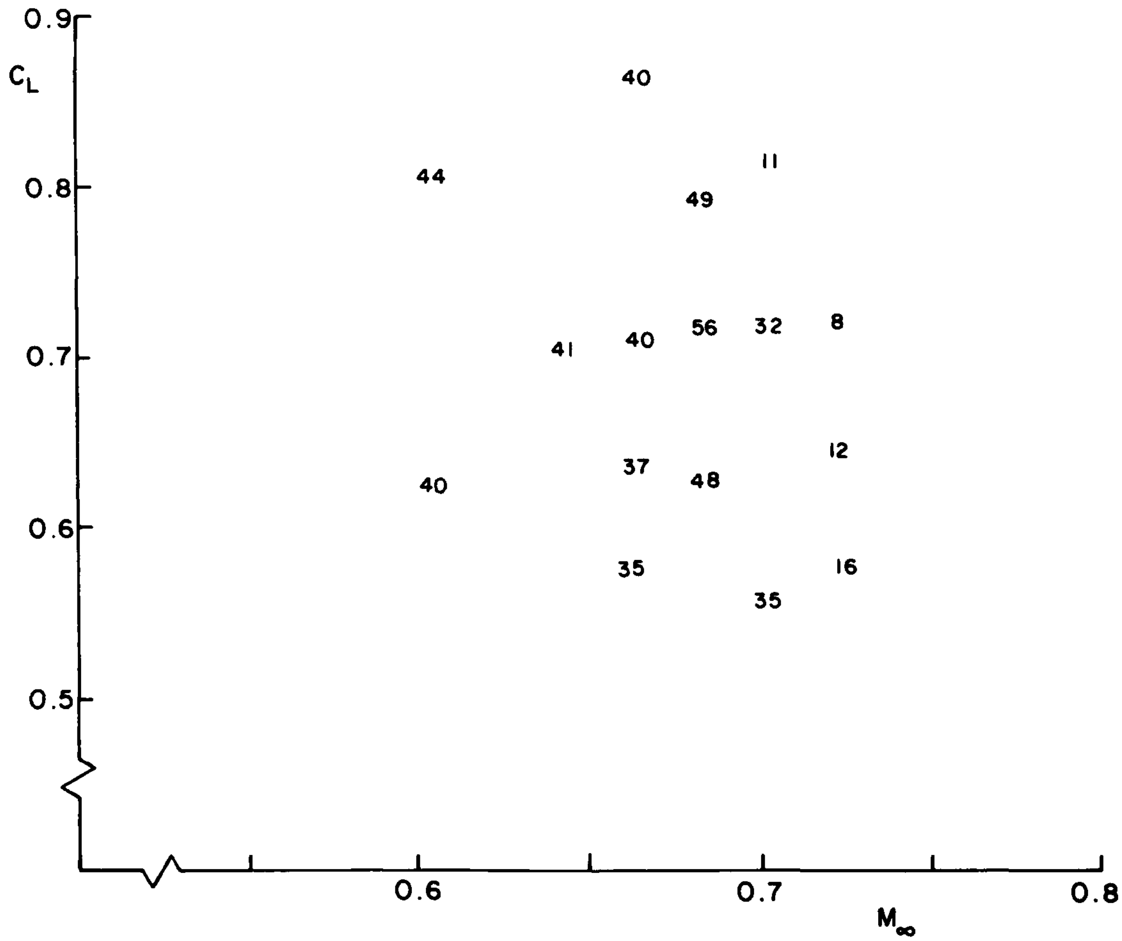

FIG. 20b: RANGE PARAMETER $M_\infty C_L/C_{D_W}$ VALUES FOR $R_c = 12.8 \times 10^6$

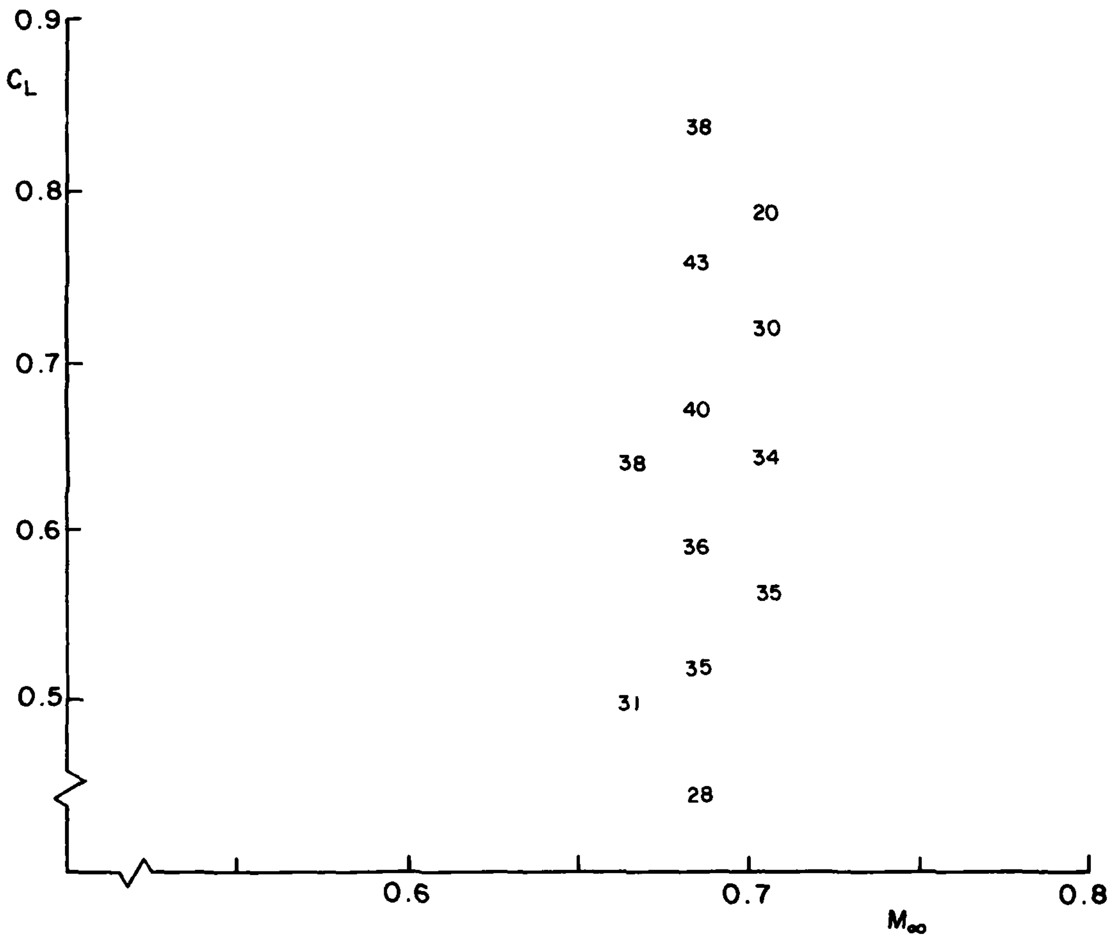

FIG. 20c: RANGE PARAMETER $M_\infty C_L/C_{D_W}$ VALUES FOR $R_c = 16.7 \times 10^6$

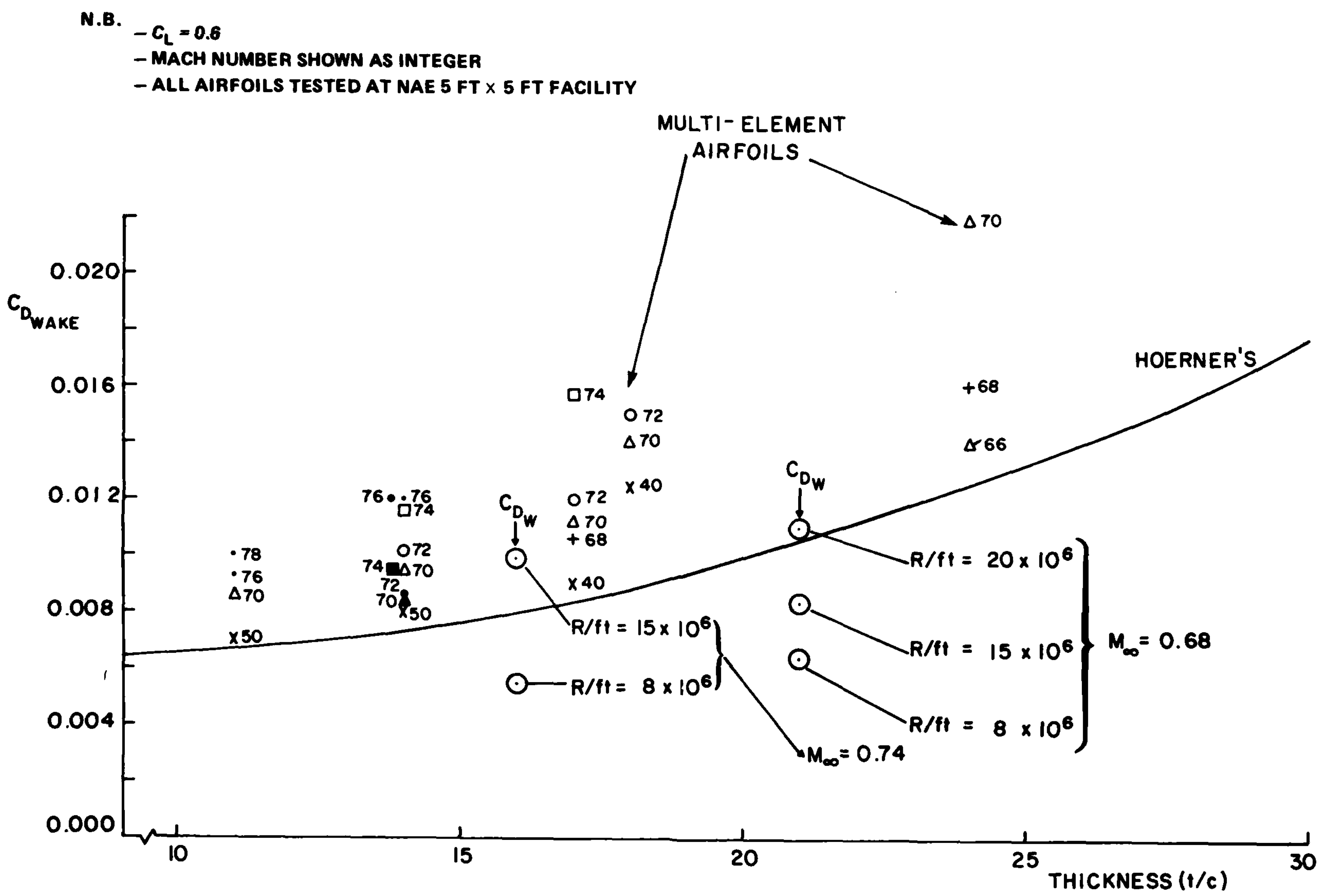

FIG. 21a: DRAG COMPARISONS WITH OTHER AIRFOILS USING C_{D_W}

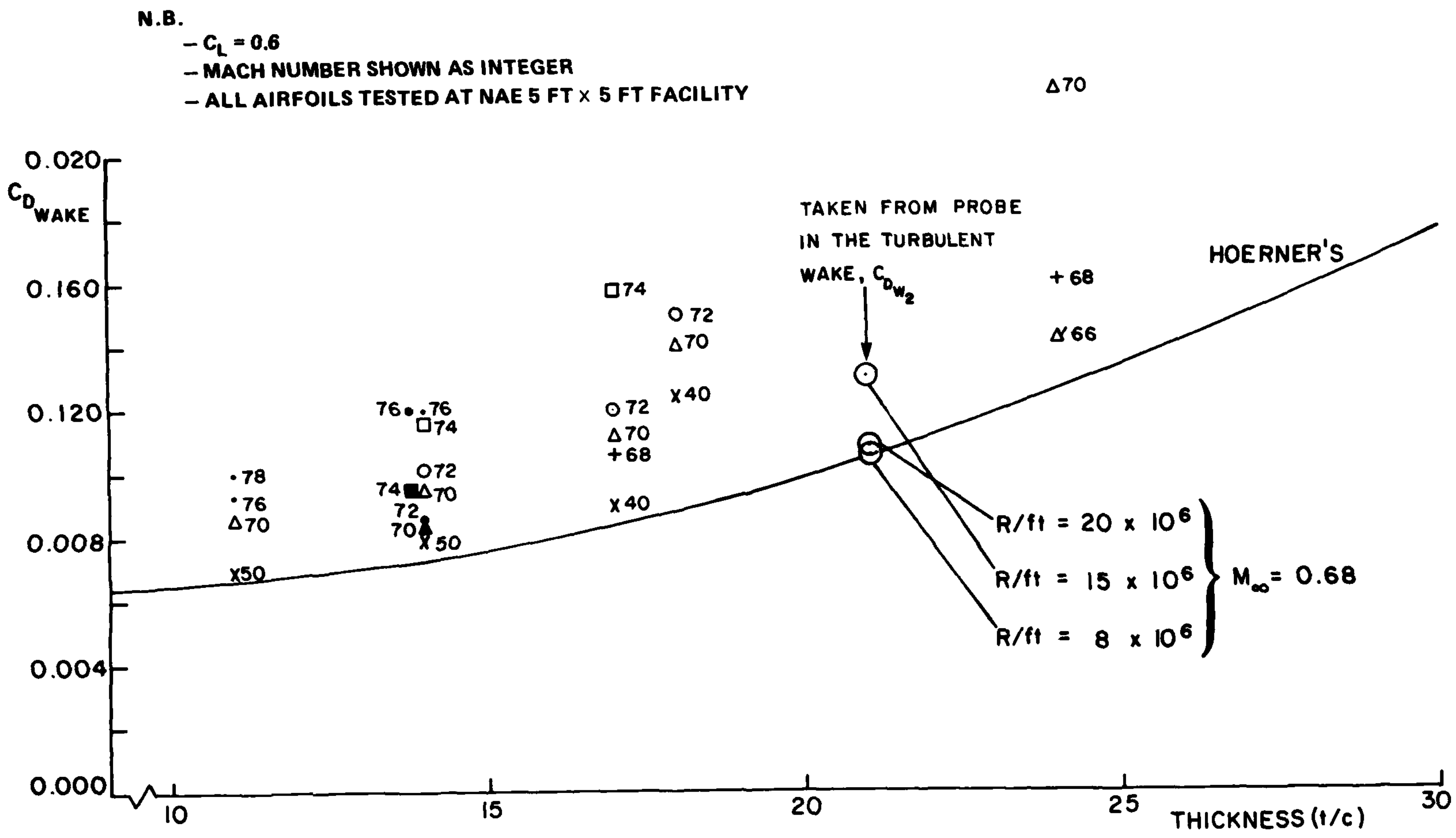

FIG. 21b: DRAG COMPARISONS WITH OTHER AIRFOILS USING $C_{D_{W_2}}$

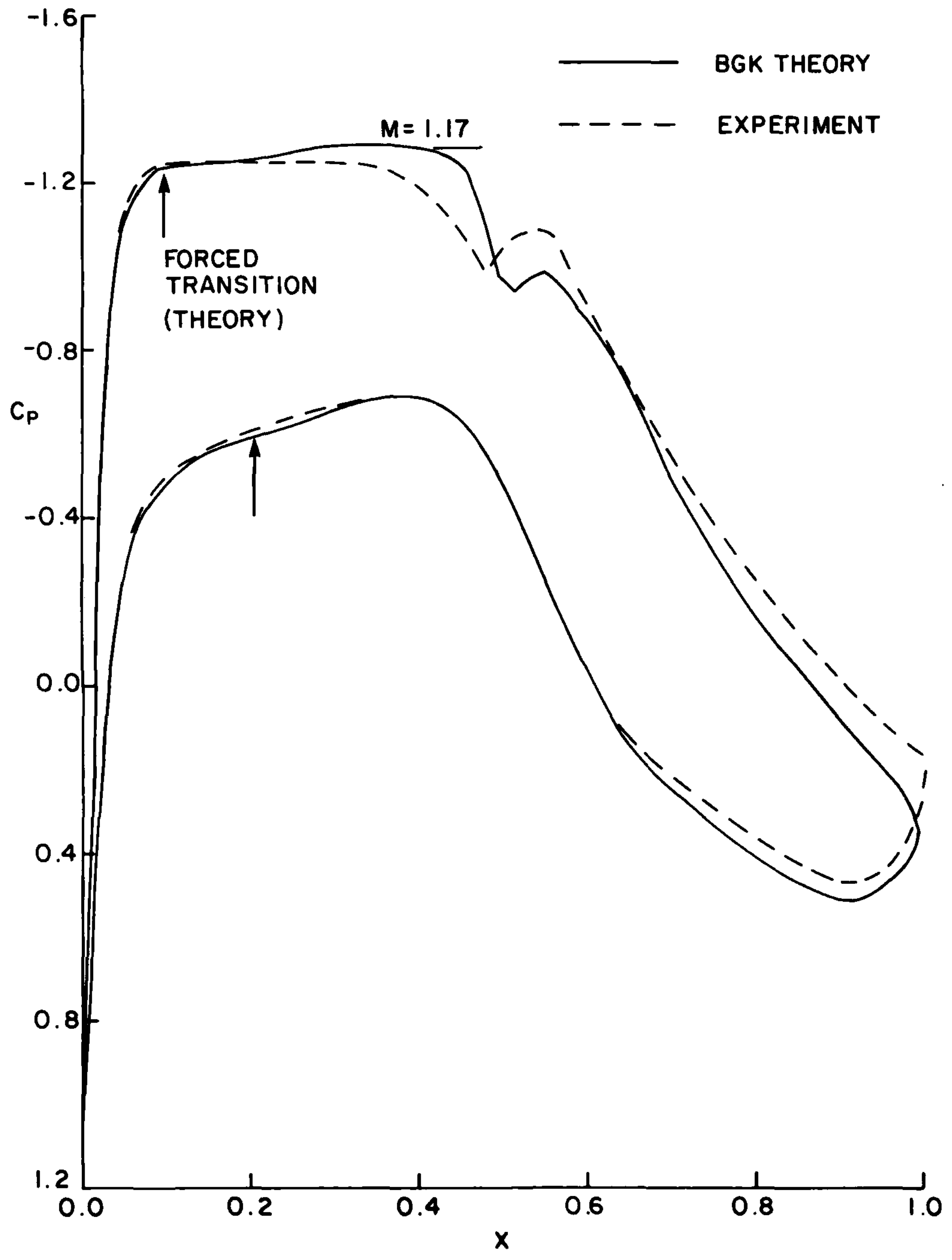

FIG. 22: COMPARISON BETWEEN THEORY AND EXPERIMENT
$M_\infty = 0.68$, $C_L = 0.623$, $R_c = 12.8 \times 10^6$

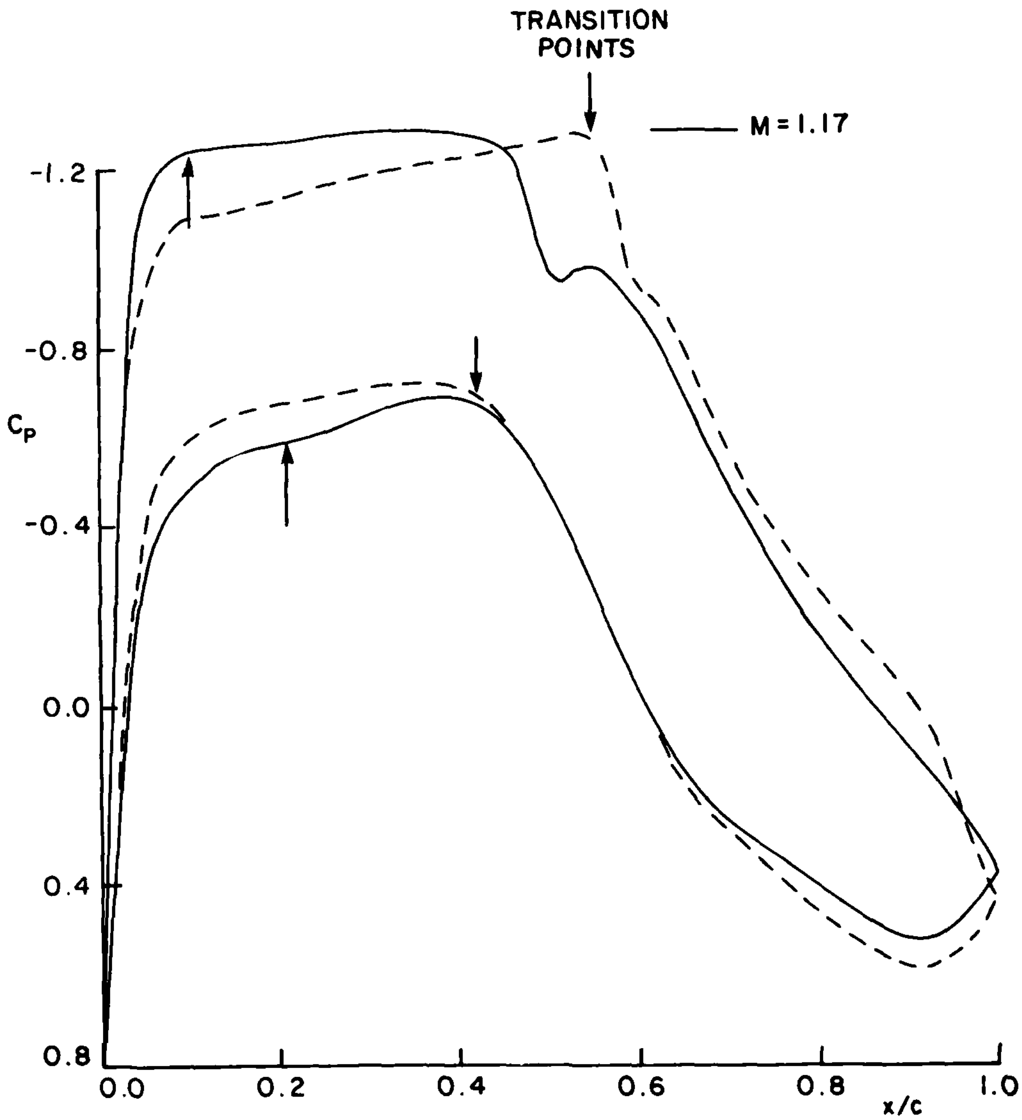

FIG. 23: TO SHOW THE EFFECT OF DIFFERENT TRANSITION POINTS ON THE BGK PRESSURE DISTRIBUTION $M_\infty = 0.68$, $C_L = 0.623$, $R_c = 12.8 \times 10^6$

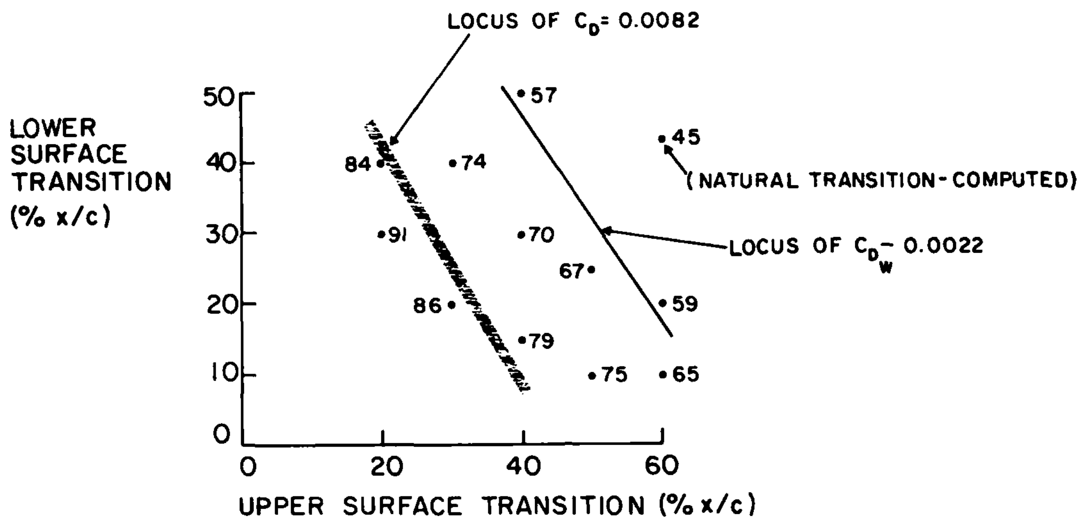

FIG. 24a: DRAG COUNT LEVELS FOR VARIOUS POSITIONS OF TRANSITION (THEORETICAL) $R_c = 12.8 \times 10^6$, $M_\infty = 0.68$, $C_L = 0.6$
EXPERIMENTAL $C_{D_W} = 0.0082$

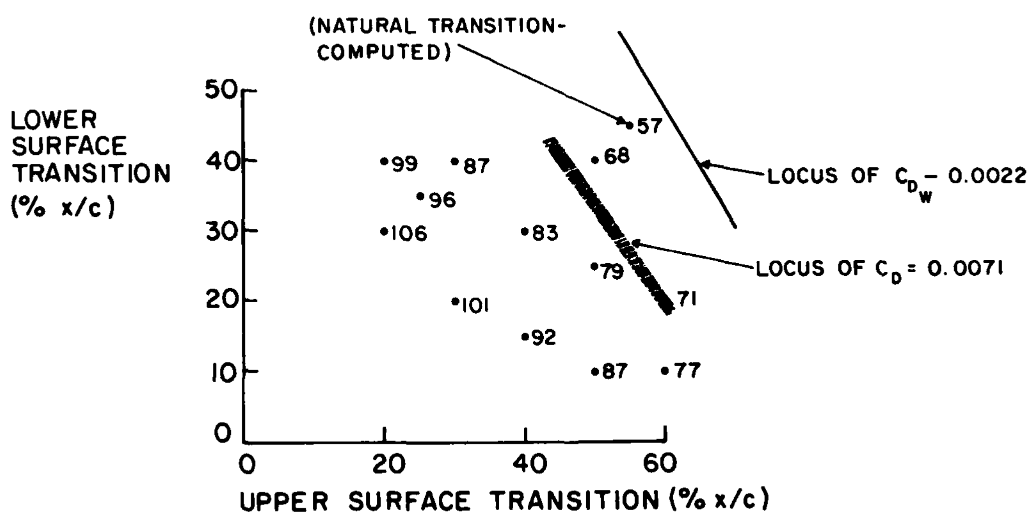

FIG. 24b: DRAG COUNT LEVELS FOR VARIOUS POSITIONS OF TRANSITION (THEORETICAL) $R_c = 6.8 \times 10^6$, $M_\infty = 0.68$, $C_L = 0.6$
EXPERIMENTAL $C_{D_W} = 0.0071$

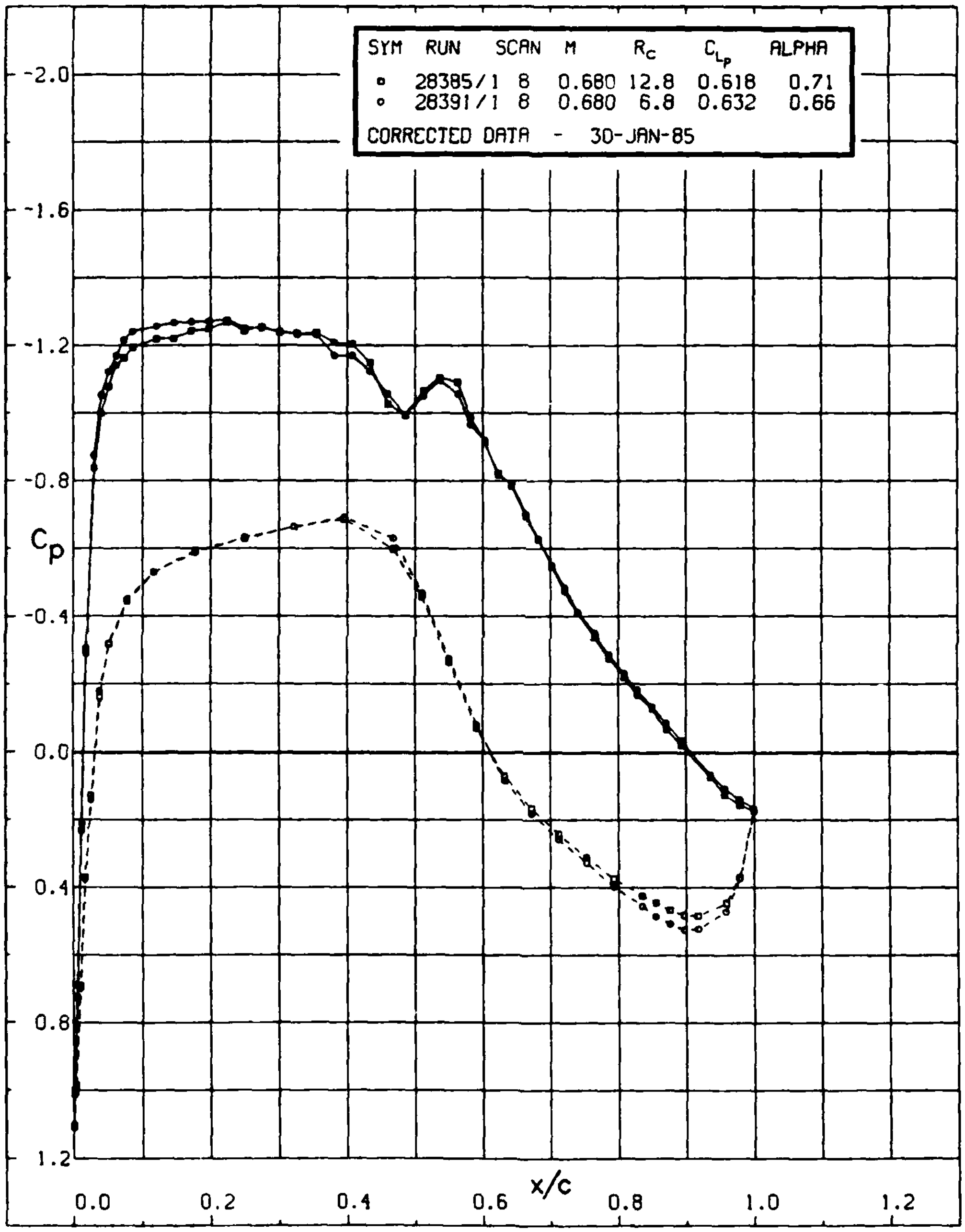

FIG. 25: EFFECT OF R_c ON THE PRESSURE DISTRIBUTION

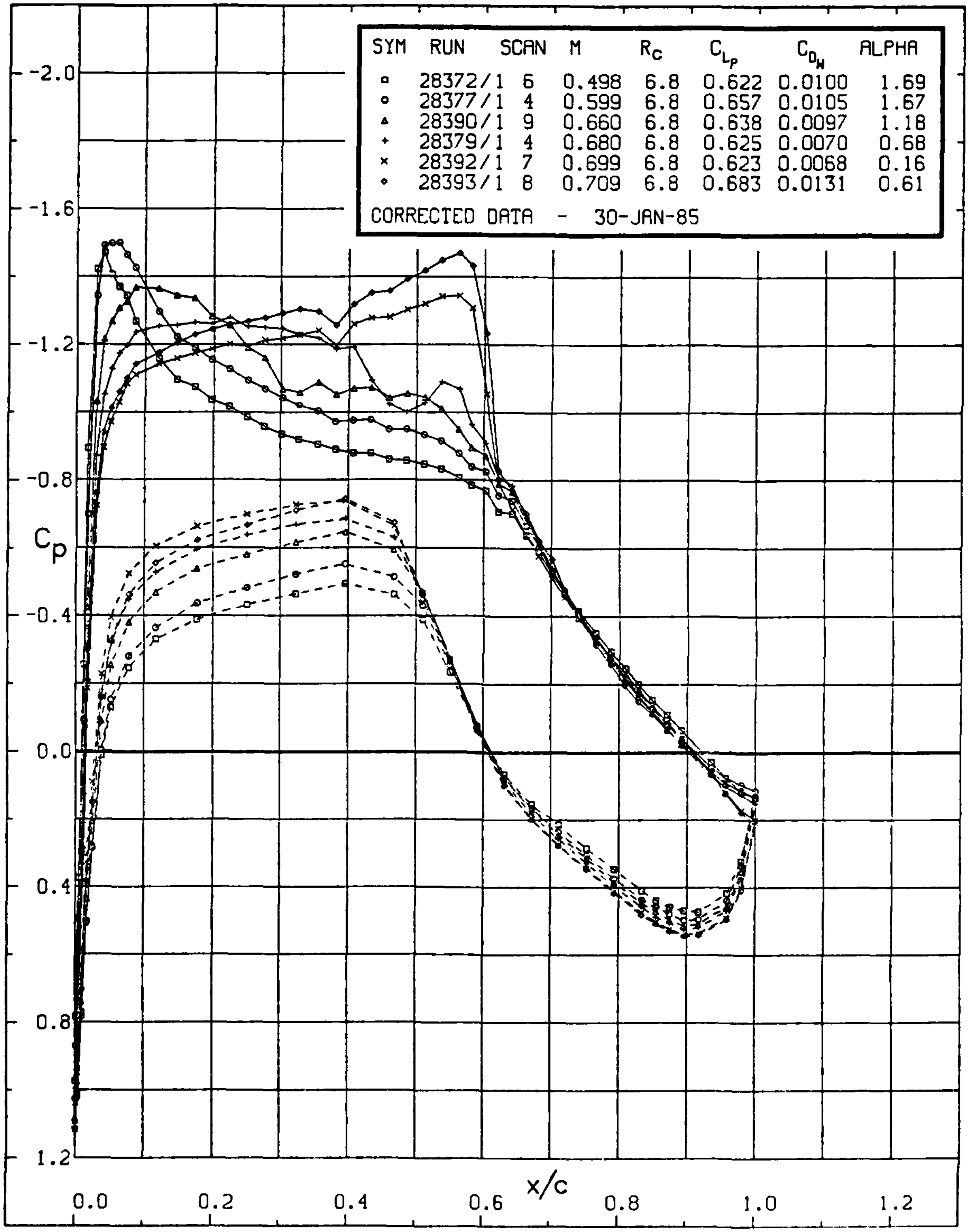

FIG. 26: EFFECT OF INCREASING M_∞ ON THE C_p DISTRIBUTION

REPORT DOCUMENTATION PAGE / PAGE DE DOCUMENTATION DE RAPPORT

REPORT/RAPPORT	REPORT/RAPPORT
NAE-AN-34 (1a)	NRC No. 25076 (1b)
REPORT SECURITY CLASSIFICATION / CLASSIFICATION DE SÉCURITÉ DE RAPPORT: Unclassified (2)	DISTRIBUTION (LIMITATIONS): Unlimited (3)

TITLE/SUBTITLE/TITRE/SOUS-TITRE

Analysis of Experimental Data for a 21% Thick Natural Laminar Flow Airfoil, NAE 68-060-21:1

4

AUTHOR(S)/AUTEUR(S)

D.J. Jones
M. Khalid

5

SERIES/SÉRIE

Aeronautical Note

6

CORPORATE AUTHOR/PERFORMING AGENCY/AUTEUR D'ENTREPRISE/AGENCE D'EXÉCUTION

National Research Council Canada
National Aeronautical Establishment — High Speed Aerodynamics Laboratory

7

SPONSORING AGENCY/AGENCE DE SUBVENTION

8

DATE	FILE/DOSSIER	LAB. ORDER COMMANDE DU LAB.	PAGES	FIGS/DIAGRAMMES
85-10			54	26
9	10	11	12a	12b

NOTES

13

DESCRIPTORS (KEY WORDS)/MOTS-CLÉS

1. Aerofoils (Low Drag)
2. Aerofoils — Wind Tunnel Testing
3. Aerofoils — Drag

14

SUMMARY/SOMMAIRE

NAE and de Havilland Aircraft of Canada have designed and tested in the NAE 5 ft X 5 ft wind tunnel a 21% thick supercritical airfoil capable of sustaining long runs of laminar flow on both surfaces. The measured drag levels are superior to those of any model previously tested in this facility and are comparable to classical NACA and modern NASA NLF airfoils.

15

END

FILMED

2-86

DTIC